Amplitude- and truncated partial-wave analyses combined: A single-channel method for extracting photoproduction multipoles directly from measured data

A. Švarc,[1,2,*] Y. Wunderlich,[3] and L. Tiator[4]

[1]*Rudjer Bošković Institute, Bijenička cesta 54, P.O. Box 180, 10002 Zagreb, Croatia*

[2]*Tesla Biotech, Mandlova 7,10000 Zagreb, Croatia*

[3]*Helmholtz-Institut für Strahlen- und Kernphysik der Universität Bonn, 53115 Bonn, Germany*

[4]*Institut für Kernphysik, Universität Mainz, D-55099 Mainz, Germany*

(Received 7 August 2020; accepted 22 October 2020; published 10 December 2020)

Amplitude- and truncated partial-wave analyses are combined into a single-channel method for extracting multipoles directly from measured data. In practice, we have created a two-step procedure which is fit to the same database: in the first step we perform an energy-independent amplitude analysis where continuity is achieved by constraining the amplitude phase, and the result of this first step is then taken as a constraint for the second step where a constrained, energy-independent, truncated partial-wave analysis is done. The method is tested on the world collection of data for η photoproduction, and the obtained fit results are very good. The sensitivity to different possible choices of amplitude phase is investigated and it is demonstrated that the present database is insensitive to notable phase changes due to an incomplete database. New measurements are recommended to remedy the problem.

DOI: 10.1103/PhysRevC.102.064609

I. INTRODUCTION

Finding a connection between QCD and experiment is a *conditio sine qua non* for establishing whether a particular description of the effects of nonperturbative QCD is close to being correct, and a lot of effort has, in the last decades, been put into doing it via comparing resonance spectra. While on the QCD side, a resonance spectrum is standardly predicted by lattice QCD and various QCD-inspired phenomenological models, on the experimental side it is standardly extracted by identifying poles of the scattering matrix [1]. However, given that resonances or poles must have definite quantum numbers, finding pole structure of experimental data must necessarily go through a partial-wave decomposition where the angular dependence at a fixed energy is represented by a decomposition over the complete set of Legendre polynomials, which then define proper eigenvalues of the angular-momentum operator. Combining good quantum numbers of angular momenta with the known spins of the reacting particles, resonance quantum numbers are fully defined. However, one should be aware that observables which are measured are most generally given in terms of amplitudes, and not partial waves, and to obtain partial waves one has to invest some extra work. Unfortunately, in that process the single-channel partial-wave decomposition turned out to be rather nonunique. For decades, it has been known that, in the single-channel case, even a complete set of observables is invariant with respect to the phase rotation of all reaction amplitudes by the same arbitrary real function of energy and angle (continuum ambiguity) [2–4], and this free rotation either causes a rearrangement of strength between real and imaginary parts of amplitudes and partial waves for energy-dependent phase-rotation functions, or it even mixes partial waves for angular-dependent phase-rotation functions. These effects lead to unacceptable discontinuities in amplitudes and partial waves, and have been extensively discussed in Refs. [5,6]. The main conclusion is that at least one of the reaction amplitude phases must be forced to be continuous in energy and angle in order to restore a continuous, unique solution. The open question is how to accomplish this task with minimal model dependence. With all these issues at hand, finding an optimal method for extracting partial waves with minimal reference to a particular theoretical model for fixing the phase turns out to be of utmost importance.

A direct consequence of the continuum ambiguity is that an unconstrained single-channel, single-energy partial-wave analysis (SE PWA), in the sense that there is absolutely no correlation among SE PWA solutions at neighboring energies, must be discontinuous. This is the consequence of the fact that, if a phase is unspecified at an isolated energy, then the free fit chooses a random phase value because there is an infinite number of phases which give an absolutely identical set of observables. So, the variation of the phase between neighboring energies may be random and discontinuous. If the variation of the phase between neighboring energies is discontinuous, the redistribution of strength between real and imaginary part at each energy will be random, so the partial wave must be discontinuous, too. The standard way of achieving the continuity was to implement it on the level of partial waves, so one resolved to constrain partial waves directly to values originating from some particular theoretical model. In

*alfred.svarc@irb.hr

this case, the model dependence is strong. The first ideas to use more general principles of analyticity for imposing the continuity instead of referring to a particular model were introduced in the mid 1980s by the Karlsruhe-Helsinki group for pion-nucleon (πN) elastic scattering in the form of fixed-t analyticity [7]. In this case instead of demanding the proximity of fit partial waves to some model values, the continuity is imposed on the level of reaction amplitudes by requiring fixed-t analyticity. In other words, the group was fitting the world collection of data requiring that the reaction amplitude for a fixed-t have a certain analytic, hence continuous form. In this way, any specific dependence on a particular model was reduced to the level of discussing what is the correct analytic structure of the reaction amplitudes, and this form is fairly well defined by the branch points of the analyzed reaction. Unfortunately, imposing analyticity in the Mandelstam t variable opened quite some additional issues, and this is extensively discussed in Ref. [8].

The aim of this work is to show that invoking analyticity in the Mandelstam t variable is not really needed and raises unwanted complications; the required continuity can be obtained by amplitude analysis (AA) in the Mandelstam s variable, and the continuity is imposed by requiring the proper analyticity of amplitude phases only. So, everything is done in the Mandelstam s variable, and by this the analysis becomes much simpler. To our knowledge, this is the first time that amplitude analysis and truncated partial-wave analysis are joined into one compact, self-sustained analysis scheme.

Let us stress that the continuum ambiguity problem, and all problems of the continuity of the phase related to it, are typical and inherent for single-channel analyses where unitarity is violated in the sense that there exists the loss of probability-flux into other channels. Unitarity equations become inequalities, and the free phase arises. However, in full coupled-channel formalisms where unitarity is at the end restored by summing up the flux in all channels, the invariance to phase rotations disappears as the phase is fixed, and uniqueness is automatically restored. However, this work analyzes only the single-channel case.

Let us also warn the reader about another aspect of PWA: the number of partial waves involved. As the partial-wave decomposition is an expansion over the complete set of Legendre polynomials, it is inherently infinite, but in practice it must be finite, so all we can talk about is a truncated PWA (TPWA). A lot of effort has recently been put into analyzing the features of a TPWA for pseudoscalar meson photoproduction [9,10]. A theoretical model was chosen, all observables were generated from this model with a fixed angular-momentum cutoff $\ell_{\max}$, and a complete set of observables generated this way was taken as input to TPWA. In that way the outcome of TPWA is known in advance, and a lot of conclusion on the symmetries and inter-relation among the thus formed pseudo observables have been drawn. Unfortunately, as this is an idealized case; most of these conclusions are not applicable for our practical purposes. Those pseudo observables generated from a model by default possess explicit properties like unrealistically high precision, continuity in energy and angle, various interdependence among observables due to finite truncation order, etc., which our real data do not necessarily have. This is in particular pronounced if the truncation order is too low. Therefore, we have to be very careful in our analysis of real data to take the truncation order high enough to avoid introducing additional, nonexisting symmetries into the analysis which may raise quite some problems. If we are careful enough, our obtained partial waves are not exact, but indeed are a good representation of the amplitude analysis representing the process.

The paper is organized as follows: the main text goes directly into media res by proposing the new fit method and showing applications to polarization data in η photoproduction in a detailed way. Discussions on the necessary background knowledge concerning the photoproduction formalism, as well as a more elaborate mathematical discussion on the motivation of the proposed novel analysis scheme, have been relegated to the Appendixes. In this way, we can present our main results quickly and concisely, while the interested reader can read the more elaborate mathematical discussion in parallel.

II. THE NOVEL APPROACH TO SINGLE-CHANNEL PARTIAL-WAVE ANALYSIS AND APPLICATION TO η PHOTOPRODUCTION

The main intention of our proposed scheme is to obtain a continuous set of partial waves, directly from experimental data, with the strongly reduced involvement of theoretical models.

The zeroth step of our procedure is to perform an unconstrained single-energy partial-wave analysis (SE PWA), namely, to fit the available set of measured data with a chosen number of partial waves at each available energy independently (at each energy the fit is independent of the neighboring energy). We know that such a process, due to the continuum ambiguities on the level of reaction amplitudes, must produce a set of partial waves that are discontinuous in energy, even for a complete set of pseudodata with very high precision. However, this procedure gives the best possible fit to the data with the chosen number of partial waves and directly measures the consistency of the data. So, this gives us a benchmark-set of values for the goodness-of-fit parameter chi squared—which we call $\chi^2_{\text{unc.}}(W)$ ("unc." for "unconstrained")—and any method of enforcing continuity of partial waves must be as close as possible to this set, but can never be better. Achieving the continuity of partial waves is, however, a demanding task. For the case of very precise pseudodata, it has been shown that the task is still relatively simple: it is enough to impose the continuity only in one amplitude phase to achieve the goal that the SE PWA becomes continuous [5]. However, for the real data we unfortunately have a serious problem. The existing set of observables is incomplete, and errors are realistic, so the situation changes drastically. Simple methods of imposing continuity on one phase only do not work anymore.

The standard way to impose continuity in discontinuous SE PWA is the penalty function methodology. The idea is to require that the solution one obtains by fitting the data at one isolated energy *simultaneously* reproduces the data *and* is also close to some continuous function. So, out of an in-

principle infinite number of solutions at isolated energy for the unconstrained SE PWA, one picks only those which are also close to a predetermined continuous penalization factor. Of course, the solution will depend on the size of the penalization coefficient. The smaller the coefficient, the more the solution will tend to reproduce the fitted data; it will be more discontinuous and it will less satisfy the penalization function. On the other hand, if one increases the penalization coefficient, the more the fit will reproduce the penalization function and be continuous, but it will less describe the fitted data. In the final limit of extremely low penalization coefficient, the fit will ideally describe the data and be discontinuous, and in the final limit of extremely big penalization coefficient, the fit will be continuous, perfectly describe the penalization function, and definitely disagree with the fitted data. The optimum lies somewhere in between.

The first, most standard approaches found in the literature were to penalize partial waves. We require that the fitted partial waves reproduce the observable $\mathcal{O}$ and are at the same time close to some partial waves taken from a theoretical model. So, for one observable we may at one fixed energy W write (for a literature example of a penalization scheme which acts on the level of partial waves, although not quite in the same way as in the definition given below, see for instance Ref. [11]):

$$\chi^2(W) = \sum_{i=1}^{N_{\text{data}}} w^i \left[\mathcal{O}_i^{\text{expt.}}(W,\Theta_i) - \mathcal{O}_i^{\text{theor.}}(\mathcal{M}^{\text{fit}}(W,\Theta_i))\right]^2 + \lambda_{\text{pen.}} \sum_{i=1}^{N_{\text{data}}} |\mathcal{M}^{\text{fit}}(W,\Theta_i) - \mathcal{M}^{\text{theor.}}(W,\Theta_i)|^2, \quad (1)$$

where

$$\mathcal{M} \stackrel{\text{def.}}{=} \{\mathcal{M}_0, \mathcal{M}_1, \mathcal{M}_2, \ldots, \mathcal{M}_j\}$$

is the generic notation for the set of all multipoles, w_i is the statistical weight, and j is the number of partial waves (multipoles). Here, $\mathcal{M}^{\text{fit}}$ are fitting parameters and $\mathcal{M}^{\text{theor.}}$ are continuous functions taken from a particular theoretical model.

In this case the procedure is strongly model-dependent.

A possibility to make the penalization function independent of a particular model was first formulated in the Karlsruhe-Helsinki (KH) πN-elastic PWA by Höhler and collaborators in the mid 1980s [7]. Instead of using partial waves, which are inherently model dependent, the penalization function was chosen to be constructed from reaction amplitudes which can be, in principle, directly linked to experimental data with only analyticity requirements imposed in the amplitude reconstruction procedure. So, Eq. (1) was changed to

$$\chi^2(W) = \chi^2_{\text{data}}(W) + \chi^2_{\text{pen}}(W),$$

$$\chi^2_{\text{data}}(W) = \sum_{i=1}^{N_{\text{data}}} w^i \left[\mathcal{O}_i^{\text{expt.}}(W,\Theta_i) - \mathcal{O}_i^{\text{theor.}}(\mathcal{M}^{\text{fit}}(W,\Theta_i))\right]^2,$$

$$\chi^2_{\text{pen}}(W) = \lambda_{\text{pen.}} \sum_{i=1}^{N_{\text{data}}} \sum_{k=1}^{N_{\text{amp}}} \left|\mathcal{A}_k(\mathcal{M}^{\text{fit}}(W,\Theta_i)) - \mathcal{A}_k^{\text{pen.}}(W,\Theta_i)\right|^2, \quad (2)$$

where $\mathcal{A}_k$ is the generic name for any kind of reaction amplitudes (invariant, helicity, transversity, ...). The amplitudes $\mathcal{A}_k(\mathcal{M}^{\text{fit}}(W,\Theta_i))$ are discontinuous ones obtained from fitted multipoles, and the amplitudes $\mathcal{A}_k^{\text{pen.}}(W,\Theta_i)$ are continuous amplitudes obtained in the penalization procedure. In this way, one is now responding to two challenges: to get reaction amplitudes which fit the data, and also to make them continuous. In the Karlsruhe-Helsinki case, this was accomplished by implementing fixed-t analyticity and fitting the database for fixed t with reaction amplitudes whose analyticity is achieved by using the Pietarinen expansion and using the obtained, continuous reaction amplitudes as penalization functions $\mathcal{A}_k^{\text{pen.}}(W,\Theta_i)$.[1] So, the first step of the KH fixed-t approach was to create the database $\mathcal{O}(W)|_{t=\text{fixed}}$ by using the measured data base $\mathcal{O}(\cos\theta)|_{W=\text{fixed}}$, and then to fit them with a manifestly analytic representation of reaction amplitudes for a fixed t. Then, the second step was to perform a penalized PWA defined by Eq. (2) in a fixed-W representation where the penalizing function $\mathcal{A}_k^{\text{pen.}}(W,\Theta_i)$ was obtained in the first step in a fixed-t representation. In that way a stabilized SE PWA was performed.

This approach was revived very recently for SE PWA of η photoproduction by the Main-Tuzla-Zagreb collaboration [8] and analyzed in detail. The basic result of that paper is that this fixed-t method works very reliably, but is rather complicated. First it required the creation of a completely new database $\mathcal{O}(W)|_{t=\text{fixed}}$ from the measured database $\mathcal{O}(\cos\theta)|_{W=\text{fixed}}$, which introduced a certain model dependence connected with the interpolation, and second it involved quite some problems with the importance of the unphysical regions.

Therefore, we propose an alternative: We also use Eq. (2), but the penalizing function $\mathcal{A}_k^{\text{pen.}}(W,\Theta_i)$ is generated by the amplitude analysis in the same, fixed-W representation, and not in the fixed-t representation. This simplifies the procedure significantly and avoids quite some theoretical assumptions on the behavior in the fixed-t representation.

We also propose a two-step process:

Step 1: Complete experiment analysis or amplitude analysis (CEA-AA) of experimental data in a fixed-W representation to generate the penalizing function $\mathcal{A}_k^{\text{pen.}}(W,\Theta_i)$.

Step 2: Perform a penalized TPWA, using Eq. (2) with the penalty function from *Step 1*.

One has to observe one very important fact: The "main event" happens in *Step 2*; *Step 1* serves only to impose continuity of *Step 2*. Therefore, the reaction amplitudes obtained in *Step 1* need not absolutely reproduce the data, it is important that they are close to the experiment, and that they are continuous. The best agreement is then achieved in *Step 2*. Of course, finding the optimal value of the penalization coefficient $\lambda_{\text{pen.}}$ is of utter importance.

A. Step 1: Complete experiment analysis or amplitude analysis

In Appendix A, we give the formalism of pseudoscalar meson photoproduction, and in Appendix B we discuss the

[1] In their case they have chosen to use invariant amplitudes.

details of CEA-AA. Out of detailed presentation of the problem we stress the most important fact: that the unconstrained CEA-AA is nonunique and discontinuous because of the continuum ambiguity. In this step, therefore, we have to achieve two goals: to find the amplitudes which achieve the best possible agreement with the data and are continuous at the same time. As we do not have a complete set of data of infinite precision at our disposal, it is by definition impossible to obtain the unique solution. We can only get the solution with errors generated by experiment; in other words these errors originate only in the uncertainty of data, and not in continuum ambiguity effects. *Step* 1 is also a two-part procedure. The best agreement with the data is achieved in the first part, and the continuity is imposed in the second part.

We adopt the following strategy:

(a) The best agreement with experiment is achieved in the unconstrained fit of the absolute values of all reaction amplitudes to the database (observe that in fitting absolute values we do not have any phases involved).
(b) The continuity of the solution is achieved by fixing the phases of all reaction amplitudes to the analytic phase of our choice.

Observe that *Step 1* is, because of part (b), a model-dependent step, but this model dependence will be additionally reduced in *Step 2*. Namely, in *Step 2* we fit the data with partial waves directly, so the phases of all reaction amplitudes are changed correcting the fact that the penalization which gives continuity is model dependent. We may safely say that the approach which is proposed here forces the phase of the final solution to be in-between the exact and the penalizing solution and to be continuous at the same time. The situation may further improve by iteration, i.e., to repeat *Step 1* with input from *Step 2* as was done in KH approach for fixed t, but the final result so far does not require that.

1. Obtaining absolute values

For obtaining absolute values it is extremely useful to use the *transversity representation*. Namely, in the transversity representation for η photoproduction, all four absolute values $|b_i|$ are determined by a set of four observables given by the unpolarized differential cross section $d\sigma/d\Omega \overset{\text{def.}}{=} \sigma_0$, the beam asymmetry Σ, the target asymmetry T, and the recoil-polarization asymmetry P (cf. Table II in Appendix A):

$$\begin{aligned}
\sigma_0 &= \frac{\rho}{2}(|b_1|^2 + |b_2|^2 + |b_3|^2 + |b_4|^2),\\
\hat{\Sigma} &= \frac{\rho}{2}(-|b_1|^2 - |b_2|^2 + |b_3|^2 + |b_4|^2),\\
\hat{T} &= \frac{\rho}{2}(|b_1|^2 - |b_2|^2 - |b_3|^2 + |b_4|^2),\\
\hat{P} &= \frac{\rho}{2}(-|b_1|^2 + |b_2|^2 - |b_3|^2 + |b_4|^2),
\end{aligned} \tag{3}$$

where $\mathcal{O}\sigma_0 \overset{\text{def.}}{=} \hat{\mathcal{O}}$ and ρ is defined in the Appendixes. Therefore, having all four observables with sufficient precision and in adequate number of angular points would enable us, up to discrete ambiguities, the unique extraction of the absolute values $|b_i|$ in SE PWA. By adequate programming (taking into account similarity of solutions at neighboring energies, one can eliminate discontinuities due to discrete ambiguities. All remaining discontinuities will be of experimental origin.

2. Determining phases

Up to this moment, our model is completely energy and angle independent and depends only on experimental data. However, results are still not continuous. Introducing analytic phases in this step produces continuity. For a single pole amplitude, the phase is smooth (in the vicinity of the pole the phase just quickly transverses through $\pi/2$ without producing any pronounced structure), but already two poles in the analyzed range produce phase interference, so some structures may be formed. In addition, we know that, in our energy range of interest, some threshold openings are present, and this will also produce a rather un-smooth phase behavior. So, at first it looks as if the phase may behave rather violently. On the other hand, we are not discussing partial waves where poles are directly visible, but reaction amplitudes which are a sum over all known resonances and thresholds, so the effect is smeared out. So, to the best of our knowledge, we can only say that phases are smooth and analytic. At this moment there is very little choice but to take the phase from a theoretical model. We have chosen the Bonn-Gatchina model solution BG2014-02 [12,13].

These phases are smooth and contain some structures which are introduced by the model. Just as an illustration, we show in Fig. 1 the phase of the b_1 amplitude. Other phases are very similar.

So, our first solution *Sol* 1 is obtained by using the theoretical BG2014-02 phases directly. Unfortunately, we do not know how strong and model dependent this assumption is.

Given that the single-spin observables $d\sigma/d\Omega$, Σ, T, and P are phase independent, and only the double-polarization observables of type beam target ($\mathcal{BT}$), beam recoil ($\mathcal{BR}$) and target recoil ($\mathcal{TR}$) are phase dependent, we may hope that this dependence is weak. Using the fact that phases are analytic functions offers us the possibility to test the size of this dependence.

First, we confirm that all transversity amplitude phases indeed are analytic functions. To do this, we fit all four phases with a two-dimensional Pietarinen expansion, a method which has not been formulated up to now. The method is based on Pietarinen expansion technique [14], but extended to two variables: energy and angle (more precisely, cosine of the angle $x := \cos\theta$). Namely, in energy dimension we use standard Pietarinen expansion, but each of the coefficients also depends on the angle. Similar as for the energy part, for the angular dependence we also assume the expansion over a complete set of functions, in this case we use Legendre polynomials. So, one gets an analytic function which is analytic in energy and angle and with the analyticity we control:

$$PT(W,\theta) = \frac{\sum_{k=0}^{N} c_k(x) Z(W)^k}{\left|\sum_{k=0}^{N} c_k(x) Z(W)^k\right|},$$

$$Z(W) = \frac{\alpha - \sqrt{W_0 - W}}{\alpha + \sqrt{W_0 - W}},$$

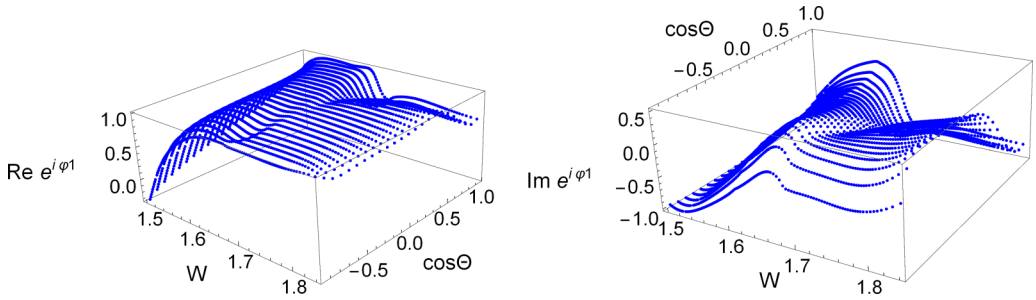

FIG. 1. The normalized transversity amplitude (phase) $e^{i\varphi_1} := b_1/|b_1|$ from the BG2014-2 solution.

$$c_k(x) = \sum_{l=0}^{M} c_{k,l} P_l(x),$$
$$x = \cos\theta, \tag{4}$$

M and N are small numbers (angular momentum index M is always around three, and energy index can vary from four for very simple energy analyticity to 20 for a fairly complicated one), $P_l(x)$ are Legendre polynomials, and α is the Pietarinen range parameter. Then we make a two-dimensional (2D) fit to the four normalized transversity amplitudes and get the coefficients α, W_0, and $c_{k,l}$ for all four absolute values.

If we are able to fit the phases with such an expansion, the phases have to be analytic functions.

We use a very simple Pietarinen expansion, with only one branch point at the η photoproduction threshold and only four terms in the angular expansion. However, we see that the analytic structure of the fitted phase is rather complicated in energy, and we need as much as $N = 20$ energy terms to obtain a decent fit. The result is shown in Fig. 2.

We again show the result only for b_1 amplitude (see Fig. 2).

The analyticity of the phases of b_1–b_4 offers us the possibility of testing the sensitivity of our method to the phase. Instead of the very physical phases b_1–b_4 of the BG2014-2 model and illustrated for b_1 in Figs. 1 and 2, we shall use a phase with much simpler analyticity, and which is generated by a 2D fit to the BG2014-02 phases with $N = 4$ terms only! This phase is again shown as an illustration for the b_1 amplitude in Fig. 3.

So, our second solution *Sol* 2 is obtained by using the smoothed theoretical BG2014-02 phases. We stress that this is a very unphysical phase because, despite being anticipated, no structures are allowed, so the amount of dissimilarity between *Sol* 1 and *Sol* 2 will give us the maximum model dependence of our assumption. It is clear that all structures in the phases in *Sol* 2 are eliminated, the obtained functions are smooth, and represent the best fit to the BG2014-02 phases.

In this way, we complete *Step 1* by using the original and smoothed analytic phases which are generated by the phases from the theoretical Bonn-Gatchina model [used phases are the best fit of BG2014-02 input with 2-D Pietarinen expansion given in Eq. (4)].

B. Step 2: Truncated partial-wave analysis

We perform a standard penalized TPWA defined by Eq. (2) with $\ell_{\max} = 5$. The only issue is finding an optimal value for the penalty-function coefficient $\lambda_{\text{pen.}}$. This issue will be discussed further below. We, however, have to discuss two features of TPWA: the threshold behavior and the database.

1. Threshold behavior

We know that, in the vicinity of a threshold, partial waves have to behave like $q(W)^L$ where $q(W)$ is the absolute value of the meson's center-of-mass (c.m.) momentum, and in our procedure that has not been enforced up to now in any way. *Step* 1 is an unconstrained fit as far as the absolute values $|b_i|$ are concerned, so no restrictions are coming through the penalty function. The TPWA itself also does not require that our result obeys that rule. Thus, we have to impose that threshold-behavior somehow.

A very natural way to do it is, again, via the penalty function technique, and we follow the method recommended by the KH group in Ref. [7]. The logic is the following: we add another penalty function to our total $\chi^2(W)$, which is to be

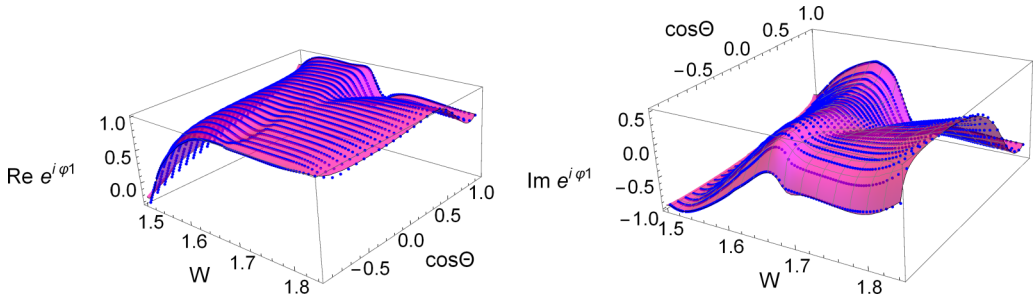

FIG. 2. The normalized transversity amplitude (phase) $e^{i\varphi_1}$ from the BG2014-02 solution (discrete symbols) and a two-dimensional Pietarinen fit (2D plane) are shown.

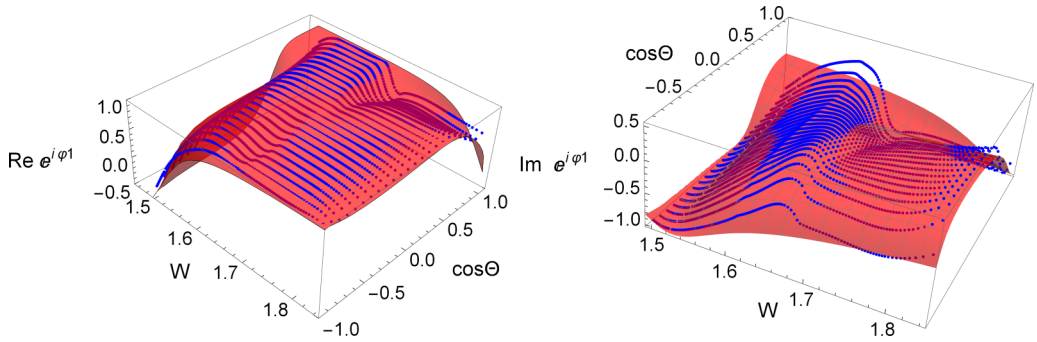

FIG. 3. The normalized transversity amplitude (phase) $e^{i\varphi_1}$ from the smoothed BG2014-02 solution.

minimized:

$$\chi^2_{\text{thr.}}(W) = \lambda_{\text{thr.}} \sum_{l=1}^{\ell_{\max}} |\mathcal{M}_{l\pm}|^2 F_{\text{thr.}}(W,b,l)^{2l},$$
$$F_{\text{thr.}}(W,b,l) = \frac{bl}{q(W)} e^{-\frac{q(W)}{0.1b}},$$
$$\mathcal{M}_{l\pm} = \{E_{l\pm}, M_{l\pm}\}, \tag{5}$$

where $F_{\text{thr.}}(W,b,l)$ is a phenomenological function instead of the theoretical function R_2^{2l} of Ref. [7], which is connected with convergence radius of the PWA expansion. We have used this function for the value $b = m_N$, where m_N is the nucleon mass, and $\lambda_{\text{thr.}} = 2$. The function $F_{\text{thr.}}(W,b,l)^{2l}$ behaves like $q(W)^{-2l}$ for small $q(W)$, and vanishes for big $q(W)$, so it scales down all multipoles with low $q(W)$ and leaves those unchanged that have a big $q(W)$. In this way, the $q(W)^l$ power law is automatically enforced for low $q(W)$.

2. Database

The data selection is particularly important as we want to be as close as possible to a complete set of observables. At this moment, we take all available measured data, and we take them without any renormalization, exactly as they are published. In Table I we give our database.

This selected set of data is somewhat specific and deserves our special attention. The set is dominated by the very dense and very precise σ_0 data from A2@MAMI, while other spin observables are measured only at 6–15 energies, and much fewer angles. So the question arises how these sparse spin data will be combined with very precise results on σ_0. We shall solve this problem via interpolation.

We generate two sets of interpolated data:

Set 1. We use all σ_0 data, and all spin data are interpolated. So the whole minimization is performed on a set which consists of σ_0 data + observables interpolated at energies and angles where σ_0 is measured. These data are marked light gray. Observe that all data are very dense, but in practice the only factually measured data are the σ_0 values, all other data are obtained by interpolation from the measured values. This set of data is somewhat model dependent, and serves only as an indication. This set will be used in *Step 1*.

Set 2. We use only part of the σ_0 data at energies where at least one additional spin observables is exactly measured. This set is not so dense in energy, but the model dependence is reduced. We denote the results corresponding to this set with red discrete symbols. This set will be used in *Step 2*.

III. RESULTS AND DISCUSSION

First we made an unconstrained fit to produce the benchmark $\chi^2_{\text{unc.}}(W)$ function, which represents the lowest possible χ^2 value for any PW fit, and consequently indicates how consistent the database actually is. However, let us remind the reader that the resulting partial waves for such a fit are random and discontinuous. Then, we performed two fits using the two-step analysis scheme introduced above, with the results being denoted as *Sol* 1 and *Sol* 2 according to the corresponding sets of b_i phases defined in Sec. II. For both solutions, we adjusted the following value for the penalty coefficient: $\lambda_{\text{pen.}} = 10$.

TABLE I. Experimental data from A2@MAMI, GRAAL, and CBELSA/TAPS used in our PWA. Data from CBELSA/TAPS are taken at the center of the energy bin.

Obs.	N	E_{lab} [MeV]	N_E	$\theta_{\text{c.m.}}$ [deg.]	N_θ	Reference
σ_0	2400	710–1395	120	18–162	20	A2@MAMI(2010) [15]
Σ	150	724–1472	15	40–160	10	GRAAL(2007) [16]
T	144	725–1350	12	24–156	12	A2@MAMI(2016) [17]
F	144	725–1350	12	24–156	12	A2@MAMI(2016) [17]
E	64	750–1450	8	29–151	8	CBELSA/TAPS(2020) [18]
P	66	725–908	6	41–156	11	CBELSA/TAPS(2020) [18]
G	48	750–1250	6	48–153	8	CBELSA/TAPS(2020) [18]
H	66	725–908	6	41–156	11	CBELSA/TAPS(2020) [18]

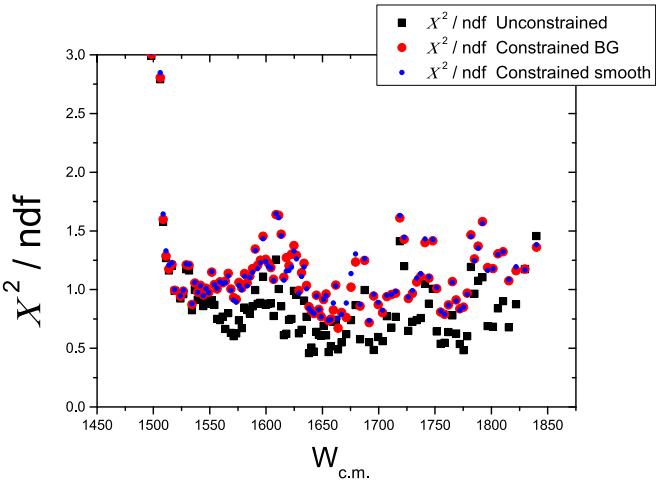

FIG. 4. A comparison of $\chi^2_{\text{unc.}}$/ndf for the unconstrained solution, as well as χ^2_{data}/ndf for *Sol* 1 and *Sol* 2 at all measured energies.

This value represents the lower boundary of the following roughly estimated optimal window of penalty-coefficient values around $\lambda_{\text{pen.}} \simeq 10, \ldots, 50$. This window of values has been determined by "sweet-spot-fitting" techniques similar in spirit, but not exactly equal, to those proposed in Secs. II and III of Ref. [19]. The coefficient for the threshold penalty (5) was set to $\lambda_{\text{thr.}} = 2$.

At this moment it is essential to show the difference between $\chi^2_{\text{unc.}}$/ndf for the unconstrained solution, as well as χ^2_{data}/ndf for *Sol* 1 and *Sol* 2 (ndf is the number of degrees of freedom). We show it in Fig. 4.

The $\chi^2_{\text{unc.}}$/ndf from the unconstrained solution has by far the smallest values; however, multipoles for this solution are discontinuous. The χ^2_{data}/ndf for both solutions *Sol* 1 and *Sol* 2 is somewhat worse, but still very good.

However, the χ^2_{data}/ndf for *Sol* 1 and *Sol* 2, solutions with two different phases, is barely distinguishable! χ^2/ndf for *Sol* 1, the solution with phase directly taken over from a very good multichannel energy-dependent (ED) model BG2014-2, is systematically better than χ^2/ndf for *Sol* 2 where the phase is *ad hoc* smoothed.[2] Somewhat more pronounced differences can be seen in the energy range 1600 MeV $\leqslant W \leqslant$ 1700 MeV, but this is exactly the area of numerous threshold openings ($K\Lambda$, $K\Sigma$, ...) where the phase is expected to have notable structure.

Therefore, we show in Figs. 5–8 the lowest multipoles for *Sol* 1 and *Sol* 2 and corresponding predictions of the BG2014-2 theoretical solution.

As expected, differences are noticeable, but not big. In spite of small differences in χ^2/ndf for *Sol* 1 and *Sol* 2, the obtained multipoles are not identical.

[2]There are several points where this is not the case, but this is just the reflection of the fact that the phase from BG2014-2 model is still only a model and not a genuine phase, so there is a possibility that smoothed phase is accidentally better.

A. *Sol* 1, solution with BG 2014-2 phase

B. *Sol* 2, solution with smoothed BG2014-2 phase

In Fig. 9 we repeat the plot of χ^2/ndf for the whole process for *Sol* 1 from Fig. 4, but in addition we give the χ^2/N_{data} for the whole fit, and χ^2/N_{data} for individual observables. The χ^2/N_{data} for individual observables is extremely important as it gives one the internal consistency of the database used. We do not show the similar figure for *Sol* 2 as two figures are practically indistinguishable.

However, the fits to the data for both solutions *Sol* 1 and *Sol* 2 are practically indistinguishable. So, in Figs. 10–17 we give the agreement of *Sol* 1 and *Sol* 2 with the fitted observables and compare it to the results of BG2014-2 solution.

Thus, we obtained almost identical fits of all observables in the present database (indistinguishable when plotted, but different below drawing precision when a detailed comparison of numbers is made) with two visibly different sets of multipoles!

If the database were more complete, the two sets of χ^2_{data}/ndf would be different between *Sol* 1 and *Sol* 2, and the we could refine *Step* 1 to include the phase fit as well, very similar as it has been done in the fixed-t analysis.[3] Thus, improving the precision of existing experiments and measuring additional observables to get missing phases is definitely needed to distinguish between the present solutions. On the basis of physics arguments, we definitely claim that *Sol* 1 is much more favorable, but, solely on the basis of measured data, *Sol* 2 cannot be excluded.

However, one thing is important: the proposed analysis-scheme is good enough to accomplish the given task staying only in a fixed-W representation.

Furthermore, Figs. 5–8 show the following:

(1) The obtained multipoles are fairly smooth and do not significantly deviate from the BG2014-02 predictions in the sense that there is no qualitative difference between the two sets of multipoles. They are of the same sign, they have similar shape, they have comparable structure. However, one sees that both solutions *Sol* 1 and *Sol* 2 have notably more structure than the energy-dependent BG2014-02 model, and that is to be expected because BG2014-2 is a multichannel model and does not ideally fit the data in one particular channel.

(2) One does see some apparent discontinuities at certain energies in certain multipoles (i.e., a "jump" in ImE_{2+} at 1687 MeV), but this is the result of inconsistencies of the data, and not of the inability of the proposed analysis scheme to enforce continuity.

[3]We could fit the theoretical BG2014-02 phases with 2D Pietarinen expansion with at least $N = 20$ terms, and then make a global, energy-dependent fit of all observables, fixing the absolute values of reaction amplitudes to the values of the present fit with only four observables and using the Pietarinen expansion coefficients as fitting parameters for improving phases. Then we would go to *Step* 2 with improved phases which are connected to BG 2014-2 values only by taking them as initial values.

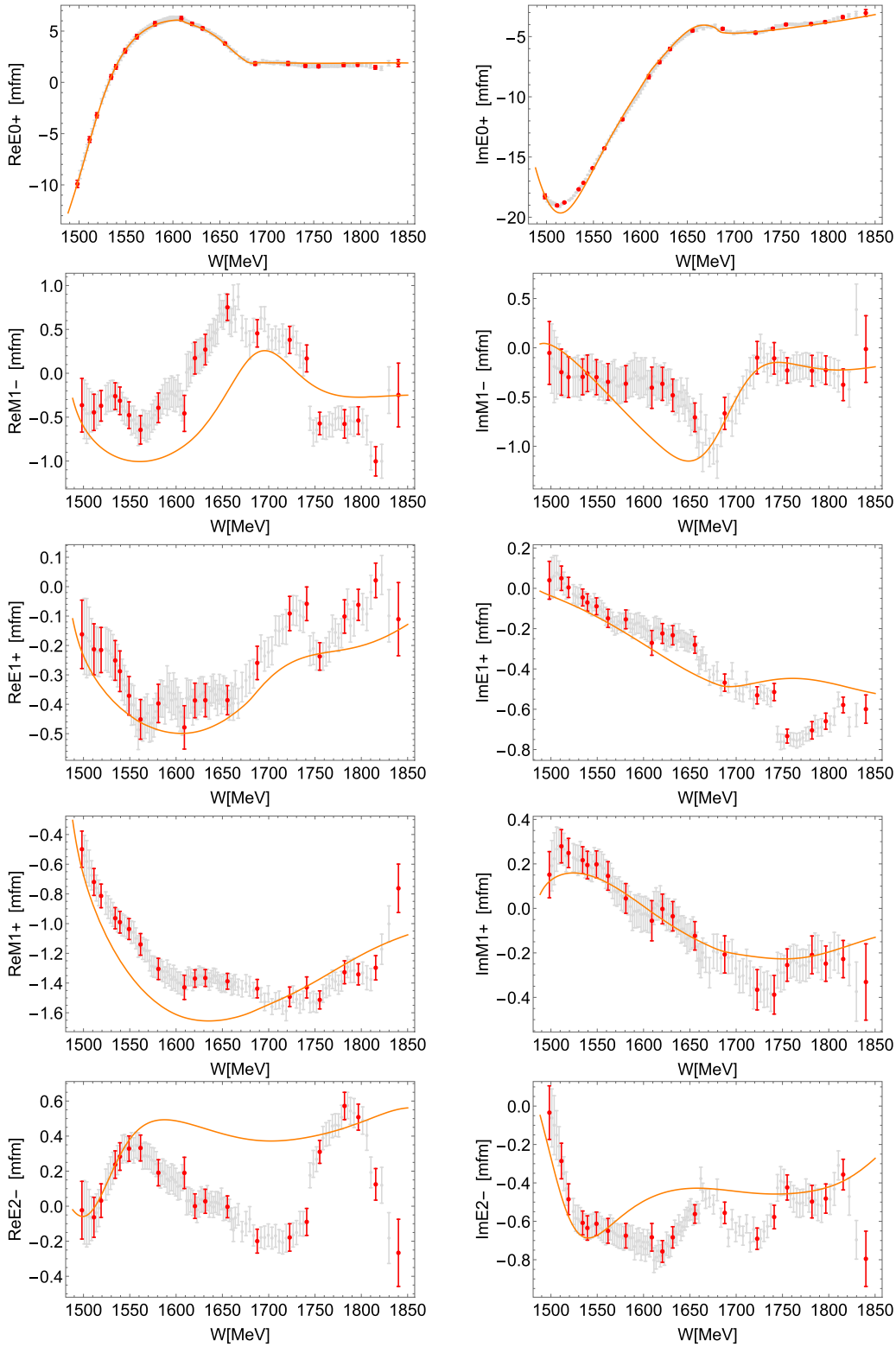

FIG. 5. Multipoles for $L = 0$, 1, and 2 partial waves for *Sol* 1. Gray discrete symbols correspond to Set 1, and red discrete symbols correspond to Set 2. Orange full line is BG2014-2 solution for comparison. Abbreviation mfm stands for millifermi.

Namely, as shown in a former publication [5], forcing the phase to be a continuous function is always resulting with continuity for the complete set of observables measured with sufficient precision (in Ref. [5], this has been shown for pseudodata with infinite precision). So, if sudden discontinuities appear, they should be solely attributed to the inconsistency in the data itself.

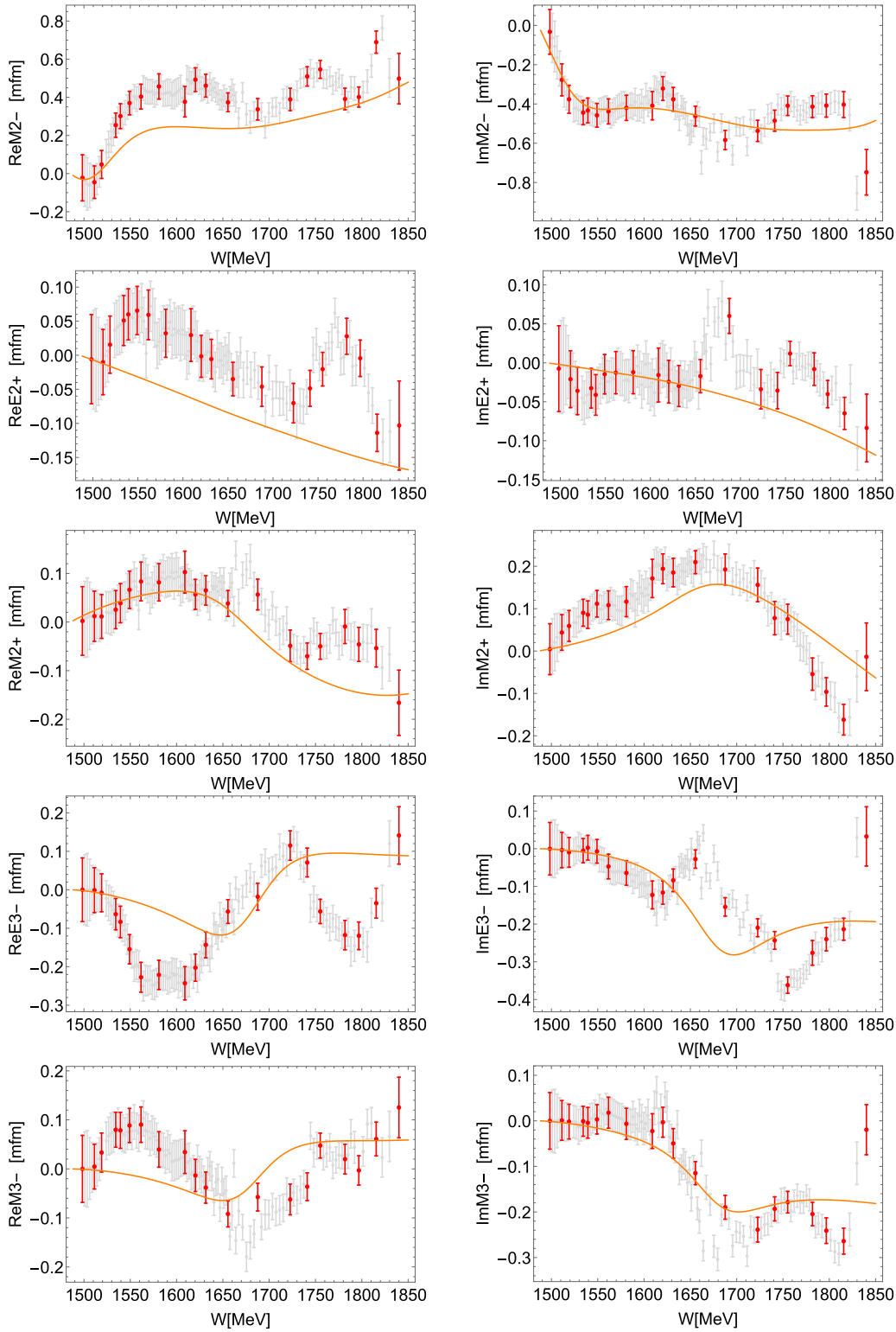

FIG. 6. Multipoles for $L = 2$ and 3 partial waves for *Sol* 1. Gray discrete symbols correspond to Set 1, and red discrete symbols correspond to Set 2. Orange full line is BG2014-2 solution for comparison. Abbreviation mfm stands for millifermi.

(3) As the low-energy behavior of the multipoles is constrained by the penalty function technique to the q^L behavior, some low-energy structure in the multipoles (mostly structures below 1550 MeV) may result from this effect. However, it is clearly visible that low-energy structures are more pronounced for *Sol* 2 which is obtained with the smoothed, nonphysical set of phases. This should and will be discussed at length

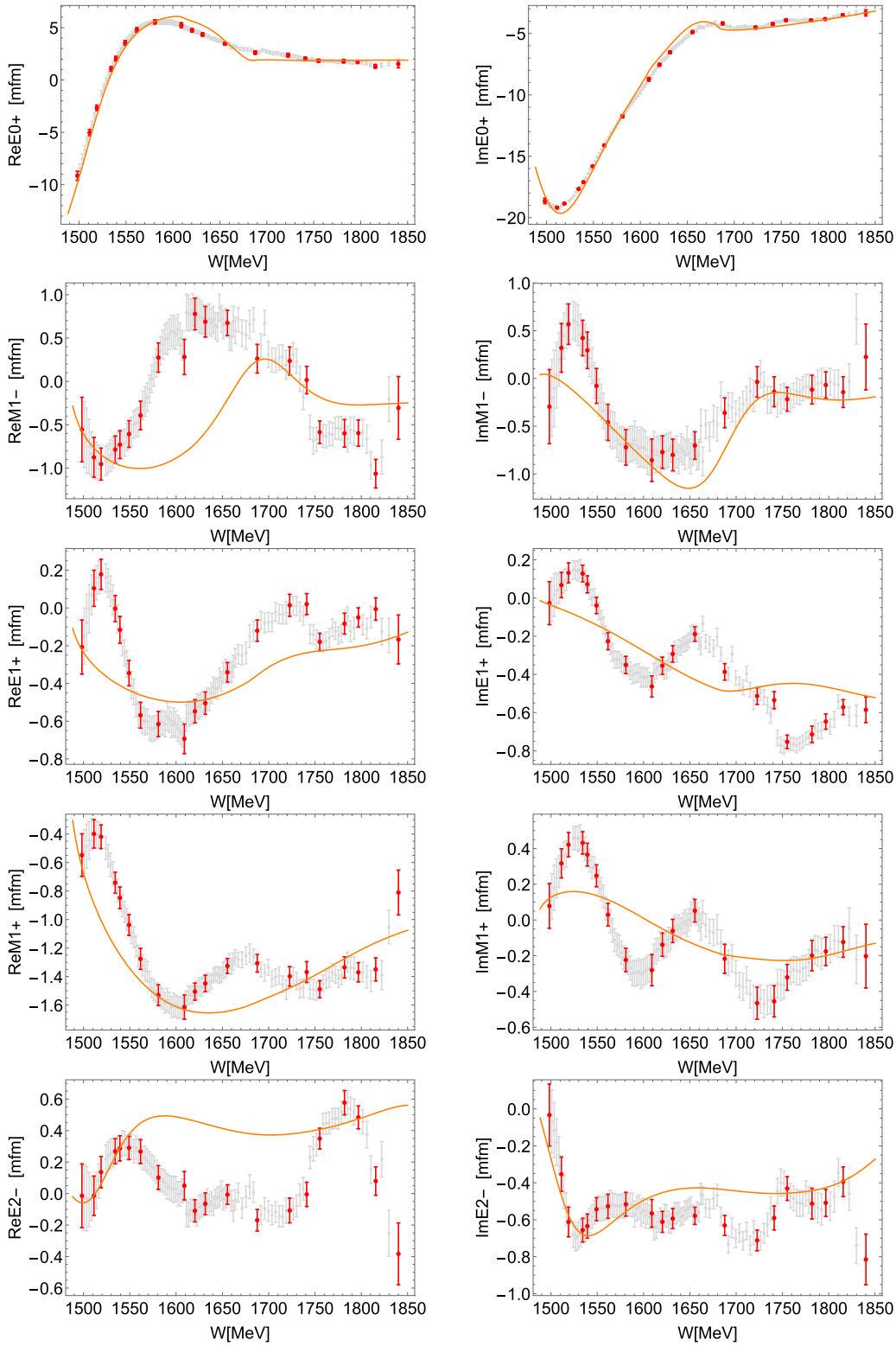

FIG. 7. Multipoles for $L = 0$, 1, and 2 partial waves for *Sol* 2. Gray discrete symbols correspond to Set 1, and red discrete symbols correspond to Set 2. Orange full line is BG2014-2 solution for comparison. Abbreviation mfm stands for millifermi.

in future research when the pole structure will be analyzed using the Laurent + Pietarinen formalism [14].

(4) We see that both sets of multipoles corresponding to different choices of interpolating techniques [Set 1 (light gray) and Set 2 (red)] are in fair agreement.

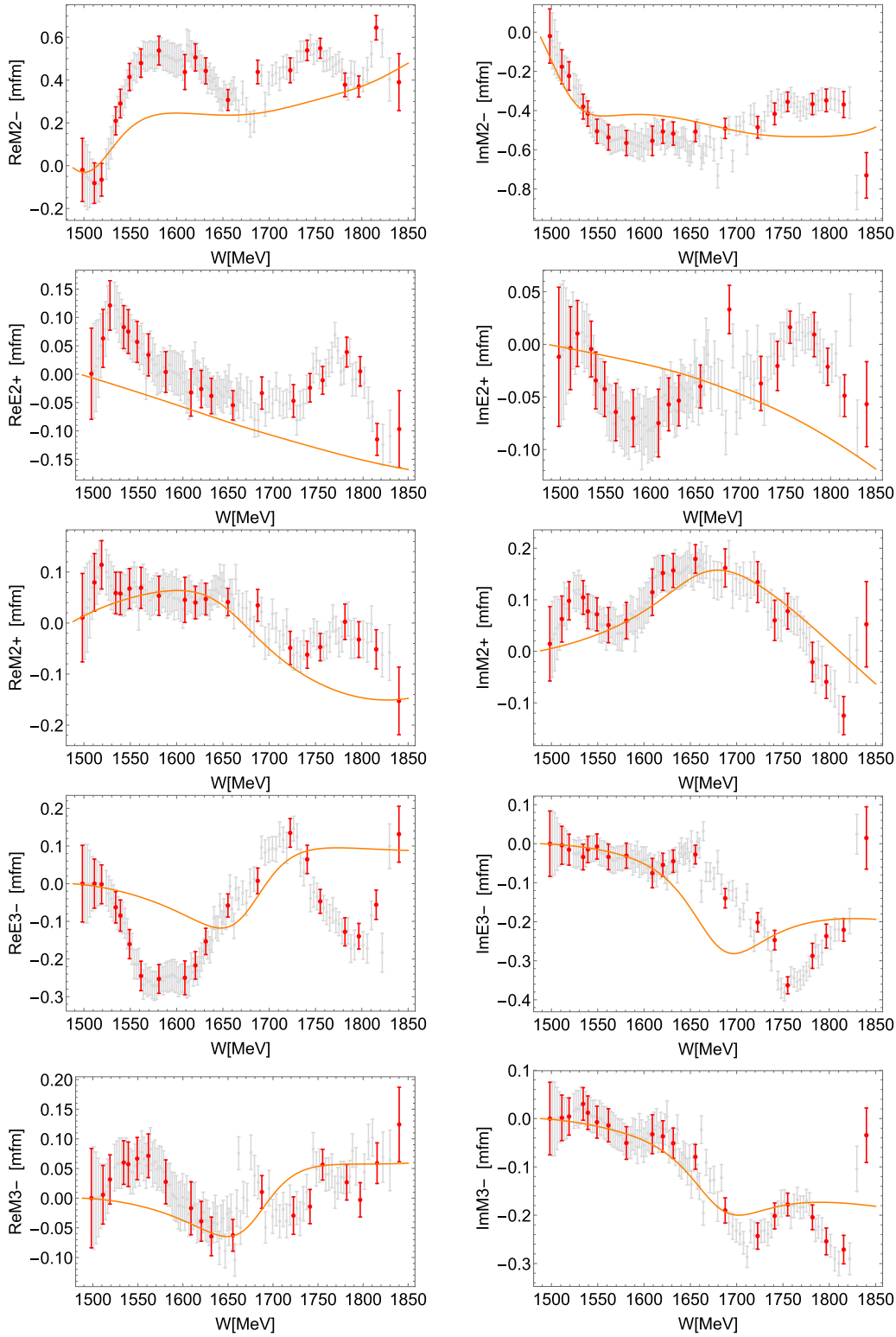

FIG. 8. Multipoles for $L = 2$ and 3 partial waves for *Sol* 2. Gray discrete symbols correspond to Set 1, and red discrete symbols correspond to Set 2. Orange full line is BG2014-2 solution for comparison. Abbreviation mfm stands for millifermi.

Figure 9 shows the following:

(1) The values of $\chi^2_{\text{data}}/\text{ndf}$ and $\chi^2_{\text{data}}/N_{\text{data}}$ are extremely good but notably nonuniform throughout the analyzed energy range. This certainly indicates inconsistencies in the data set, as will be discussed later.

(2) The distributions of $\chi^2_{\text{data}}/N_{\text{data}}$ values for particular observables differ notably.

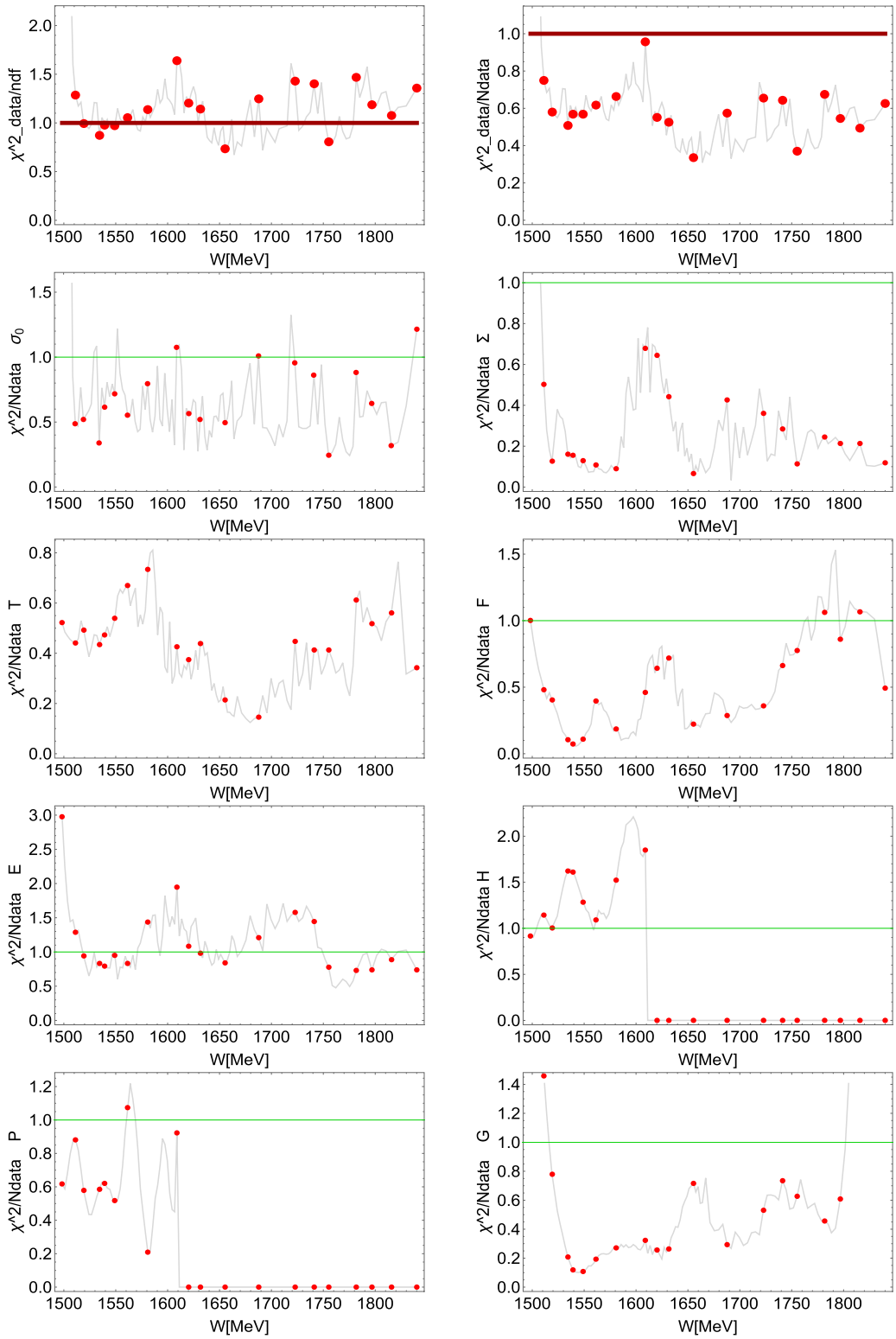

FIG. 9. χ^2/N_{data} for *Sol* 1.

(a) It is uniform and very good (close to 0.5) in the complete energy range for σ_0.
(b) It is very good and close to 0.5 in most of the energy range for Σ, T, F, and G, but each of the observables show energy ranges where this quantity suddenly increases:
(i) For F it rises from an average value in the ranges 1600–1650 and 1750–1840 MeV; much more for the second range.
(ii) For T it jumps only slightly at lower and higher energies.

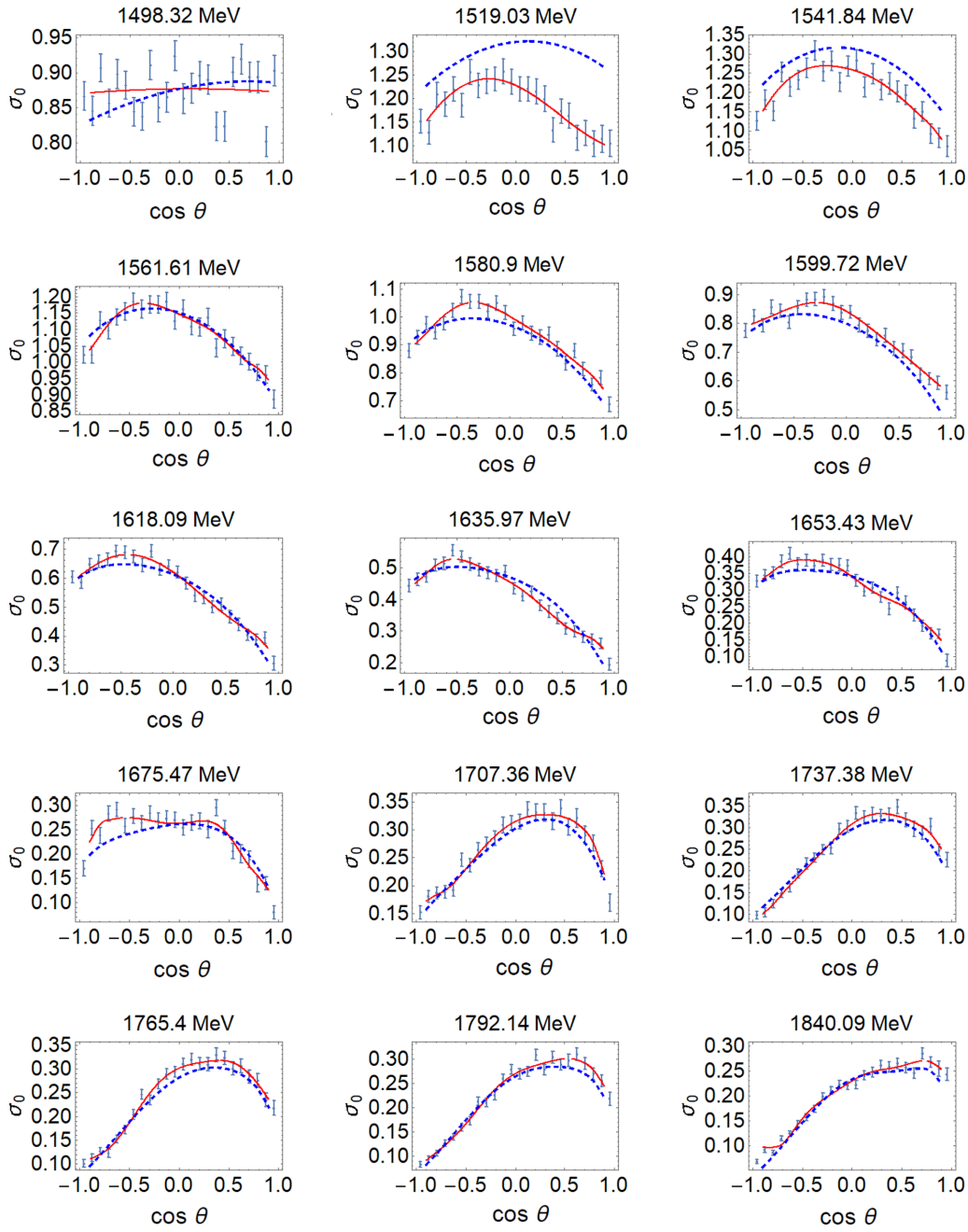

FIG. 10. Comparison of experimental data for σ_0 (discrete symbols) with results of *Sol* 1 (red full line) and BG2014-2 fit (blue dashed line) at representative energies.

(iii) For G it also jumps in the ranges 1600–1650 and 1750–1840 MeV.

(c) It is uniform in the whole energy range, but somewhat worse than typical for E.

(d) It is somewhat worse for P in the available energy range 1500–1650 MeV.

(e) It notably worse for H in the complete measured energy range 1500–1650 MeV.

(3) The quantities in these figures indicate that there exist certain inconsistencies among measured data in certain energy ranges. In particular, H seems to deviate in the complete measured range and F seem to be problematic at higher energies.

In Figs. 10–17 we compare the quality of fit of *Sol* 1 and the theoretical BG014-02 model for all experimental data from Table I. We conclude that the quality of fit for *Sol* 1 is much better than the one of BG2014-02, and this is not surprising as this is a fit, and BG2014-02 is an energy-dependent microscopic model. In addition, we have made some tests, and we strongly suspect that the agreement with the data given in Fig. 9 cannot be better even for the free fit. So, this solution

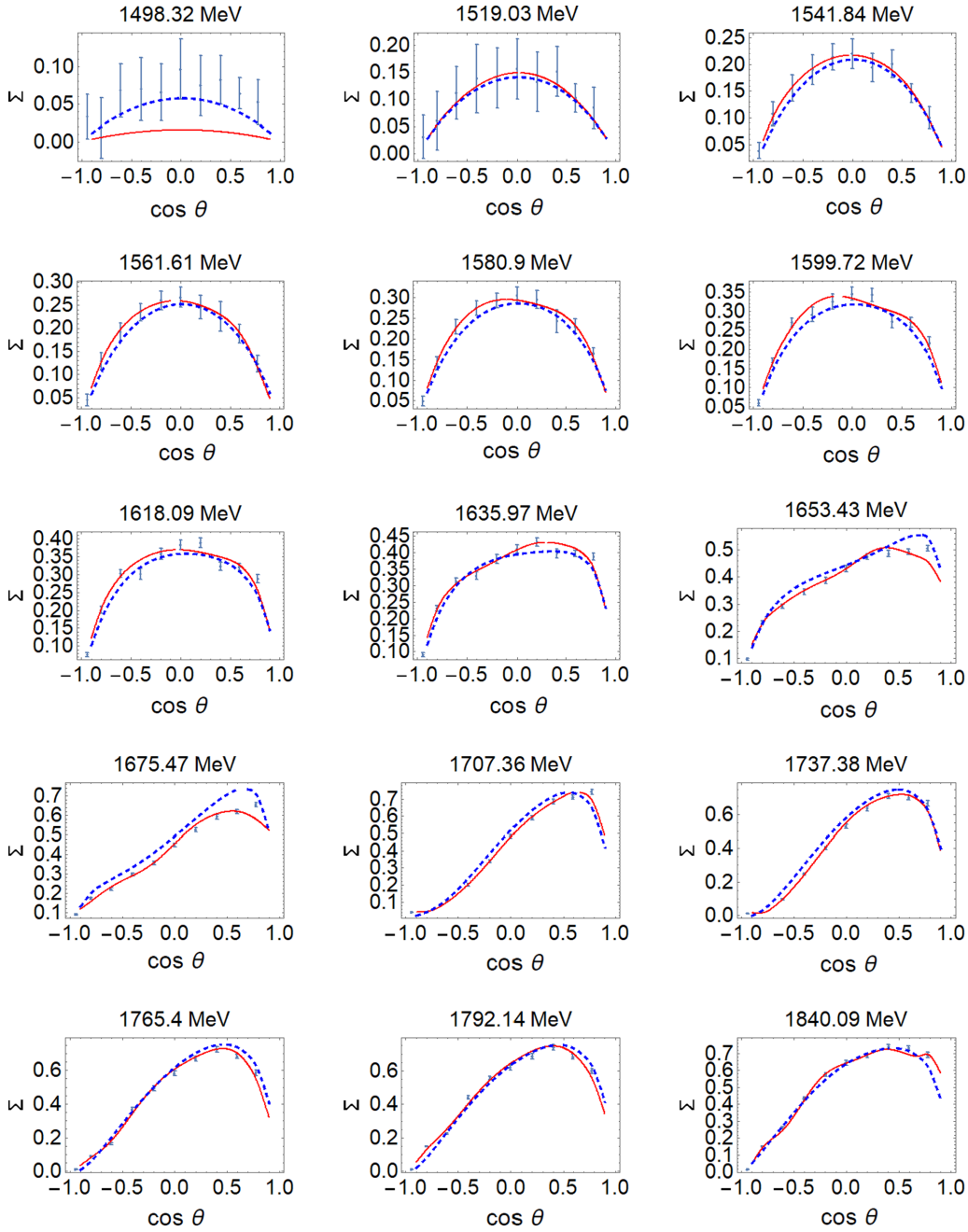

FIG. 11. Comparison of experimental data for Σ (discrete symbols) with results of *Sol* 1 (red full line) and BG2014-2 fit (blue dashed line) at representative energies.

is very close to the best result one can achieve. However, analyzing the details of these figures one can also trace the angular and energy ranges which are problematic and have either big dissipation or big uncertainty, and we can very confidently predict where a particular observable is expected to be. The need for new measurements is automatically suggested. Immediately, we may recommend that H and F should be remeasured towards the end of the measured energy range. In addition, the energy range of the P and H observable is much smaller, so we recommend to extend the energy range to at least 1800 MeV.

IV. SUMMARY AND CONCLUSIONS

In this paper we have presented a new data analysis scheme for single-channel pseudoscalar meson photoproduction. It combines the amplitude analysis CEA-AA of a complete experiment with the truncated partial-wave analysis TPWA of an idealistic case, where all higher partial waves that cannot be fit would be completely negligible.

The strength of our scheme is its simplicity and strongly reduced reference to any particular theoretical model. But it is also robust enough that it can always extend the lack of data by additional theoretical constraints.

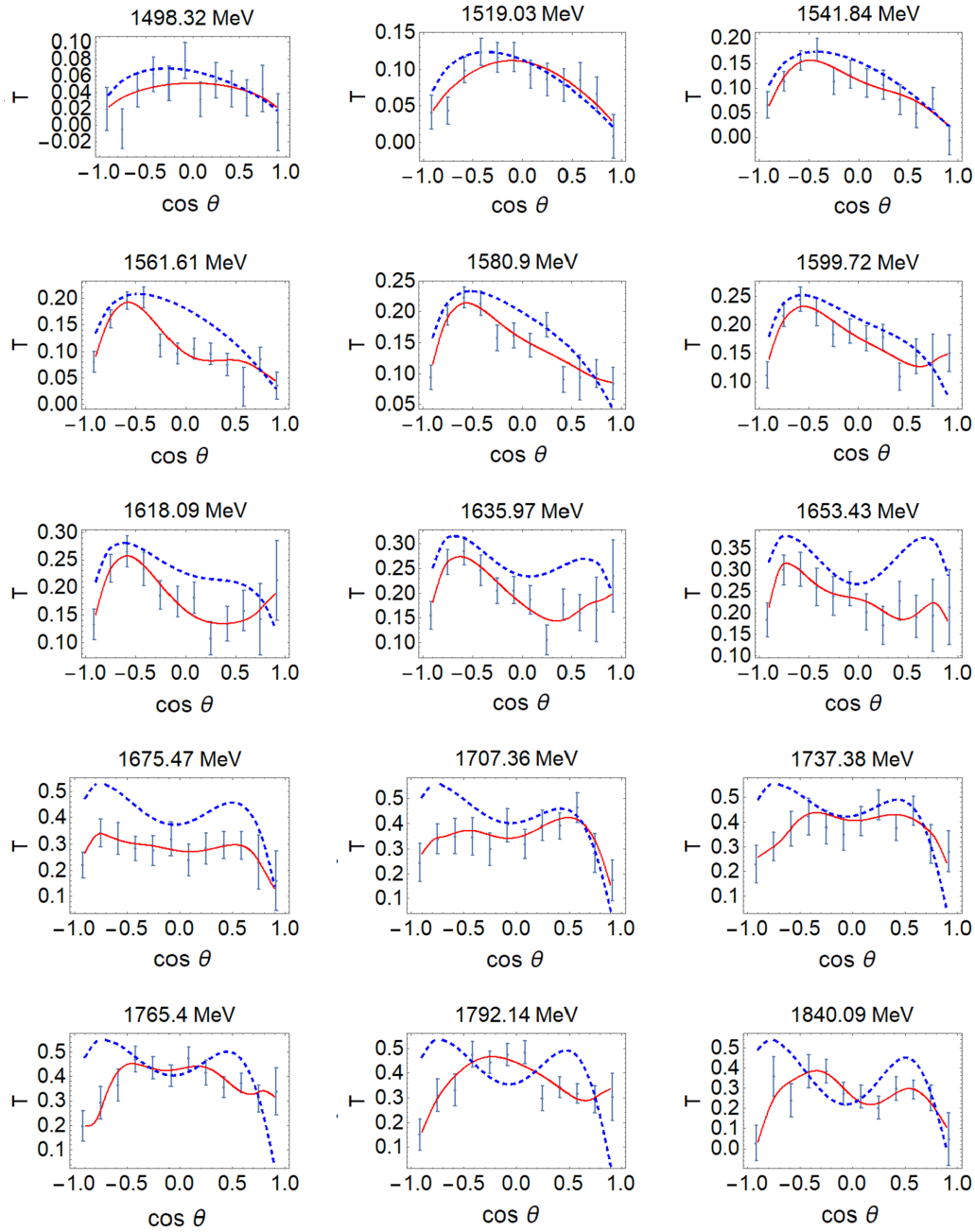

FIG. 12. Comparison of experimental data for T (discrete symbols) with results of *Sol* 1 (red full line) and BG2014-2 fit (blue dashed line) at representative energies.

The possible weaknesses of the scheme are that it requires a lot of experimental data, and that they should be measured with considerable reliability. The main opportunities of the method are that it enables the direct extraction of resonance parameters via Laurent-Pietarinen formalism [14], and at the same time gives a direct possibility to check the consistency of measured data sets. The scheme also allows us to test the importance of certain observable to the final result.

The proposed fit-method yields a continuous and reliable set of partial waves without experiencing a strong influence to any theoretical model.

The new variable P, measured by the Bonn group [18], is extremely important because it helps to pin down the absolute values of the transversity amplitudes in *Step 1*.

The present data set is insufficient to uniquely determine the reaction amplitude phase, so as an example we generate two solutions with almost identical quality of the fit to the data, but with notably different partial waves. More measurements are needed if one wants to better specify the pole structure of partial-wave solutions.

Fitting the relative phase with present database is futile. New measurements of well selected observables can improve the analysis a lot. With them the analysis scheme can be

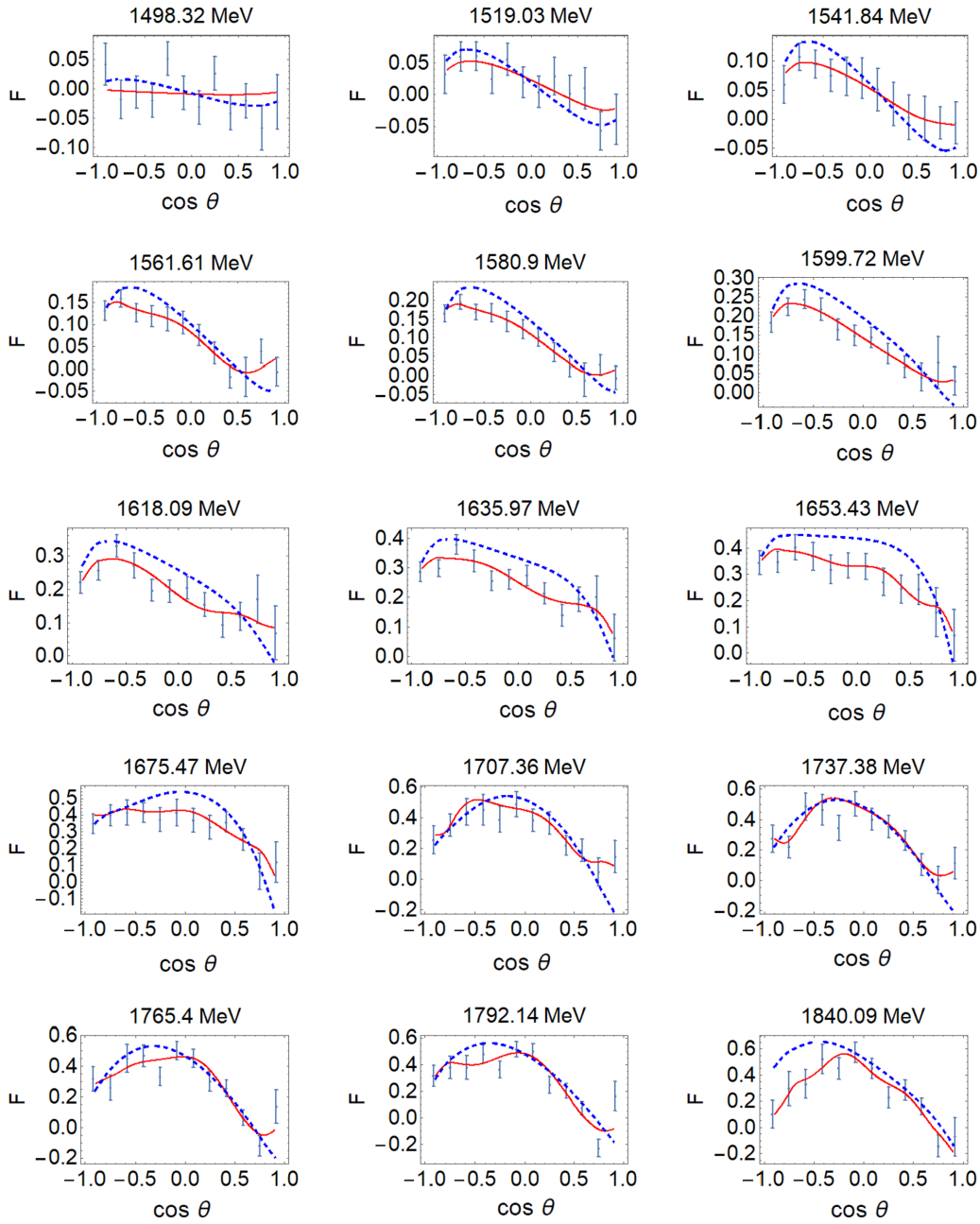

FIG. 13. Comparison of experimental data for F (discrete symbols) with results of *Sol* 1 (red full line) and BG2014-2 fit (blue dashed line) at representative energies.

extended to include fitting the relative phase too, so a unique solution could be generated.

The method offers the possibility to directly analyze the internal consistency of different data sets, avoiding the influence of different theoretical models.

The separate analysis of χ^2/N_{data} for eight polarization observables in Fig. 9 suggest that certain observables should be remeasured in certain energy ranges, and Figs. 10–17 imply the ranges where the consistent data are expected to be.

We believe that the central result of our work consists of the fact that applying CEA-AA in practical data analyses is a very important technique, which should be employed more and more in the future. The problem of the CEA-AA has been mostly studied as an isolated mathematical problem in the past, yielding the well-known complete sets of eight observables. However, the CEA-AA is also quickly applied to real data and it is a numerically quite well-behaved procedure, due to the fact that it involves only four complex numbers for all energies. The real power of the CEA-AA results emerges once they are combined with the TPWA. There, they have a great constraining power and make the TPWA an analysis which is known to be very badly behaved on its own for the higher ℓ_{max}, a lot more stable. Using the CEA-AA in such a constructive way, we have been able to derive SE PWA solutions for η photoproduction, which have quite controlled and small discontinuities in their energy dependence,

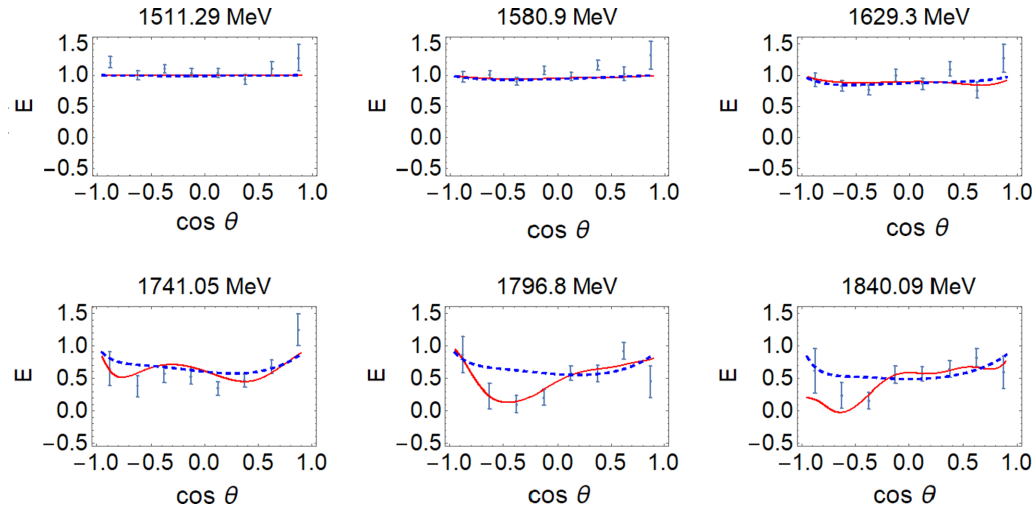

FIG. 14. Comparison of experimental data for E (discrete symbols) with results of *Sol* 1 (red full line) and BG2014-2 fit (blue dashed line) at measured energies.

even for the "small" multipoles (i.e., all multipoles other than E_{0+}).

APPENDIX A: PHOTOPRODUCTION FORMALISM

In the following, we collect all aspects of the general photoproduction formalism needed for this work. We consider a $2 \to 2$-reaction with a spin-1 photon and a spin-$\frac{1}{2}$ target nucleon in the initial state and a pseudoscalar meson and a spin-$\frac{1}{2}$ baryon in the final state:

$$\gamma(p_\gamma; m_\gamma) + N\big(P_i; m_{s_i}\big) \longrightarrow \varphi(p_\varphi) + B\big(P_f; m_{s_f}\big). \tag{A1}$$

In this expression, the four-momentum as well as the variables necessary to label the spin-states have been indicated for each particle. For the reaction of η photoproduction studied in this work, the pseudoscalar φ is the η and the recoil-baryon B is the nucleon N. However, other combinations are also possible.

In the following, we collect the customary definitions for the Mandelstam variables s, t, and u. Using four-momentum conservation, $p_\gamma + P_i = p_\varphi + P_f$, each of these variables can be written in two equivalent forms:

$$s = (p_\gamma + P_i)^2 = (p_\varphi + P_f)^2, \tag{A2}$$

$$t = (p_\gamma - p_\varphi)^2 = (P_f - P_i)^2, \tag{A3}$$

$$u = (p_\gamma - P_f)^2 = (P_i - p_\varphi)^2. \tag{A4}$$

Since all particles in the initial- and final state of the reaction (A1) are assumed to be on the mass shell, the whole reaction can be described by two independent kinematic invariants. The latter are often chosen to be the pair (s, t).

In case center-of-mass (CMS) coordinates are adopted, the following relations can be established between (s, t) and the center-of-mass energy W and scattering angle θ of the reaction

$$s = W^2, \tag{A5}$$

$$t = m_\varphi^2 - 2k\sqrt{m_\varphi^2 + q^2} + 2kq\cos\theta. \tag{A6}$$

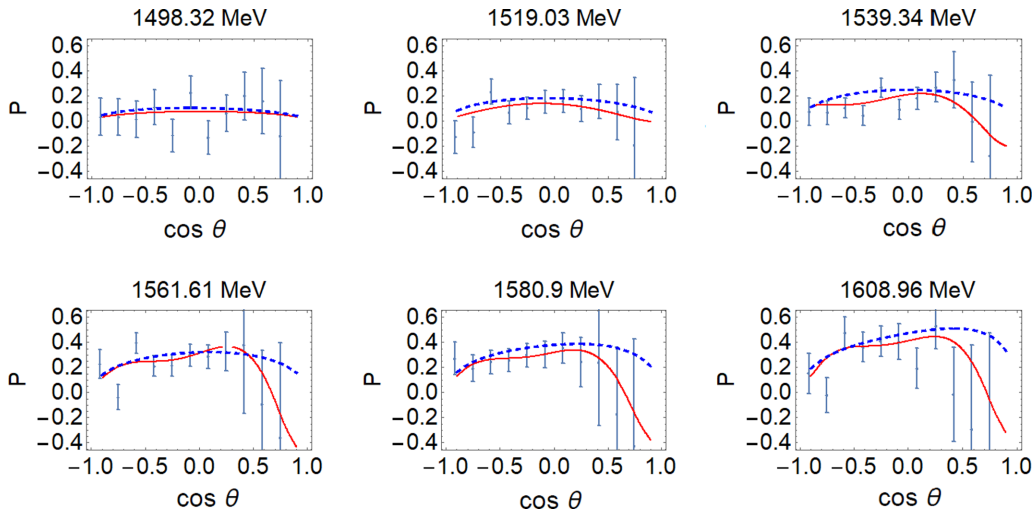

FIG. 15. Comparison of experimental data for P (discrete symbols) with results of *Sol* 1 (red full line) and BG2014-2 fit (blue dashed line) at measured energies.

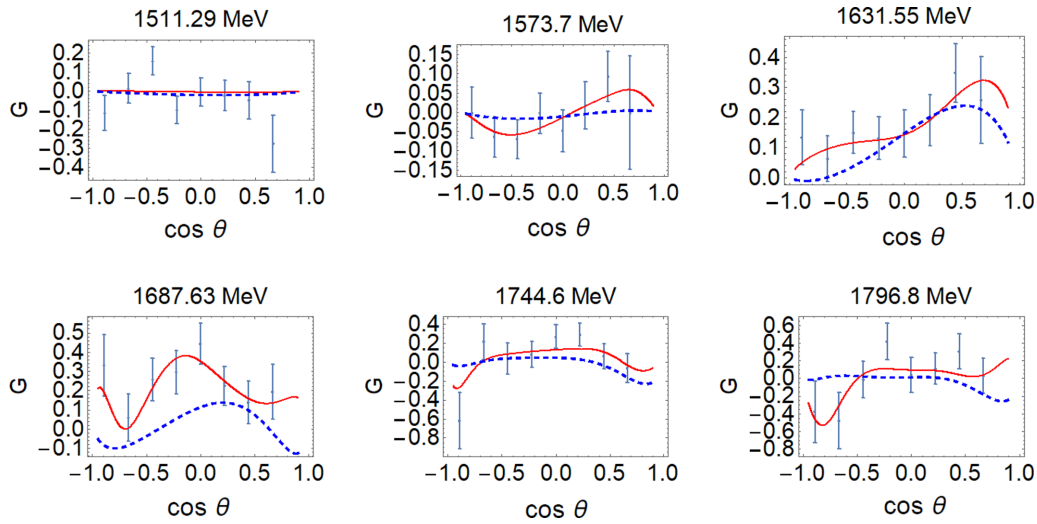

FIG. 16. Comparison of experimental data for G (discrete symbols) with results of *Sol* 1 (red full line) and BG2014-2 fit (blue dashed line) at measured energies.

Here, k and q are the absolute values of the CMS three-momenta for the photon and the meson, respectively. Both of these variables can be expressed in terms of W and the masses of the initial- and final-state particles. Therefore, it is seen that the reaction can be described equivalently in terms of (W, θ). Furthermore, the phase-space factor for the considered $2 \to 2$ reaction is defined as $\rho = q/k$.

The spins of the particles in the initial and final states of photoproduction (A1) imply a general decomposition for the reaction amplitude. This decomposition has been found by Chew, Goldberger, Low, and Nambu (CGLN) [20] and it reads:

$$\mathcal{F} = \chi^{\dagger}_{m_{s_f}} (i\vec{\sigma} \cdot \hat{\epsilon} F_1 + \vec{\sigma} \cdot \hat{q}\vec{\sigma} \cdot \hat{k} \times \hat{\epsilon} F_2 + i\vec{\sigma} \cdot \hat{k}\hat{q} \cdot \hat{\epsilon} F_3 + i\vec{\sigma} \cdot \hat{q}\hat{q} \cdot \hat{\epsilon} F_4) \chi_{m_{s_i}}. \tag{A7}$$

Here, $\hat{k}$ and $\hat{q}$ are normalized CMS three-momenta, $\hat{\epsilon}$ is the normalized photon polarization-vector, and $\chi_{m_{s_i}}$, $\chi_{m_{s_f}}$ are Pauli spinors. The complex amplitudes $F_1, \ldots, F_4$ depend on (W, θ) and are called CGLN amplitudes. Once this set of four amplitudes is determined, the full dynamics of the process is known.

The axis of spin quantization chosen for the initial-state nucleon and the final-state baryon in the decomposition (A7) coincides with the $\hat{z}$ axis in the CMS. However, other choices are also feasible, which then lead to different but equivalent systems composed of four spin amplitudes. For instance, it is possible to introduce so-called *transversity amplitudes* $b_1, \ldots, b_4$ by rotating the spin-quantization axis to the direction normal to the so-called reaction plane. The latter is defined as the plane spanned by the CMS three-momenta $\vec{k}$ and $\vec{q}$. Using the conventions employed implicitly in the work of Chiang and Tabakin [21], one arrives at the following set of

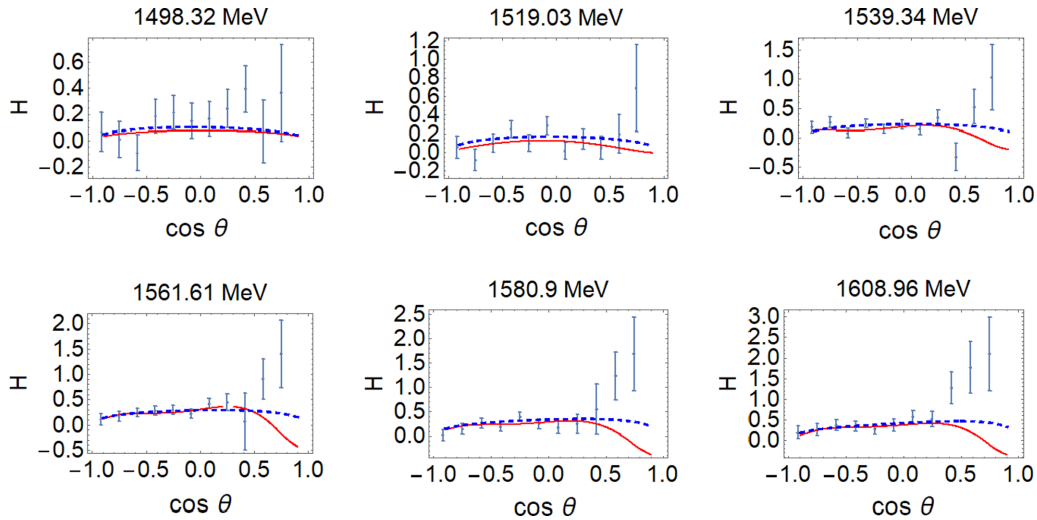

FIG. 17. Comparison of experimental data for H (discrete symbols) with results of *Sol* 1 (red full line) and BG2014-2 fit (blue dashed line) at measured energies.

linear and invertible relations between transversity and CGLN amplitudes:

$$b_1(W,\theta) = -b_3(W,\theta) - \frac{1}{\sqrt{2}}\sin\theta\left[F_3(W,\theta)e^{-i\frac{\theta}{2}} + F_4(W,\theta)e^{i\frac{\theta}{2}}\right], \tag{A8}$$

$$b_2(W,\theta) = -b_4(W,\theta) + \frac{1}{\sqrt{2}}\sin\theta\left[F_3(W,\theta)e^{i\frac{\theta}{2}} + F_4(W,\theta)e^{-i\frac{\theta}{2}}\right], \tag{A9}$$

$$b_3(W,\theta) = \frac{i}{\sqrt{2}}\left[F_1(W,\theta)e^{-i\frac{\theta}{2}} - F_2(W,\theta)e^{i\frac{\theta}{2}}\right], \tag{A10}$$

$$b_4(W,\theta) = \frac{i}{\sqrt{2}}\left[F_1(W,\theta)e^{i\frac{\theta}{2}} - F_2(W,\theta)e^{-i\frac{\theta}{2}}\right]. \tag{A11}$$

The transversity basis greatly simplifies the definitions of polarization observables (see further below) and is therefore generally used as a starting point for the discussion of complete-experiment problems. Due to these mathematical advantages, this basis is also used in the discussion in the main text (Sec. II).

To extract information on the properties of resonances, one has to analyze partial waves. In this work, we adopt the well-known expansion of the CGLN amplitudes into electric and magnetic multipoles, which reads [20,22]:

$$F_1(W,\theta) = \sum_{\ell=0}^{\infty}\{[\ell M_{\ell+}(W) + E_{\ell+}(W)]P'_{\ell+1}(\cos\theta) + [(\ell+1)M_{\ell-}(W) + E_{\ell-}(W)]P'_{\ell-1}(\cos\theta)\}, \tag{A12}$$

$$F_2(W,\theta) = \sum_{\ell=1}^{\infty}[(\ell+1)M_{\ell+}(W) + \ell M_{\ell-}(W)]P'_{\ell}(\cos\theta), \tag{A13}$$

$$F_3(W,\theta) = \sum_{\ell=1}^{\infty}\{[E_{\ell+}(W) - M_{\ell+}(W)]P''_{\ell+1}(\cos\theta) + [E_{\ell-}(W) + M_{\ell-}(W)]P''_{\ell-1}(\cos\theta)\}, \tag{A14}$$

$$F_4(W,\theta) = \sum_{\ell=2}^{\infty}[M_{\ell+}(W) - E_{\ell+}(W) - M_{\ell-}(W) - E_{\ell-}(W)]P''_{\ell}(\cos\theta). \tag{A15}$$

The multipoles can be assigned to definite conserved spin-parity quantum numbers J^P. In particular, resonances with spin $J = |\ell \pm \frac{1}{2}|$ couple to the multipoles $E_{\ell\pm}$ and $M_{\ell\pm}$.

The multipole expansion of the CGLN amplitudes F_i is formally inverted by the following well-known set of projection integrals [10,23]:

$$M_{\ell+} = \frac{1}{2(\ell+1)}\int_{-1}^{1}dx\left[F_1P_\ell(x) - F_2P_{\ell+1}(x) - F_3\frac{P_{\ell-1}(x) - P_{\ell+1}(x)}{2\ell+1}\right], \tag{A16}$$

$$E_{\ell+} = \frac{1}{2(\ell+1)}\int_{-1}^{1}dx\left[F_1P_\ell(x) - F_2P_{\ell+1}(x) + \ell F_3\frac{P_{\ell-1}(x) - P_{\ell+1}(x)}{2\ell+1} + (\ell+1)F_4\frac{P_\ell(x) - P_{\ell+2}(x)}{2\ell+3}\right], \tag{A17}$$

$$M_{\ell-} = \frac{1}{2\ell}\int_{-1}^{1}dx\left[-F_1P_\ell(x) + F_2P_{\ell-1}(x) + F_3\frac{P_{\ell-1}(x) - P_{\ell+1}(x)}{2\ell+1}\right], \tag{A18}$$

$$E_{\ell-} = \frac{1}{2\ell}\int_{-1}^{1}dx\left[F_1P_\ell(x) - F_2P_{\ell-1}(x) - (\ell+1)F_3\frac{P_{\ell-1}(x) - P_{\ell+1}(x)}{2\ell+1} - \ell F_4\frac{P_{\ell-2}(x) - P_\ell(x)}{2\ell-1}\right]. \tag{A19}$$

In these projection equations, one has $x = \cos\theta$. Polarization observables in pseudoscalar meson photoproduction are generically defined as dimensionless asymmetries among differential cross sections for different beam, target, and recoil polarization states:

$$\mathcal{O} = \frac{\beta\left[\left(\frac{d\sigma}{d\Omega}\right)^{(B_1,T_1,R_1)} - \left(\frac{d\sigma}{d\Omega}\right)^{(B_2,T_2,R_2)}\right]}{\sigma_0}. \tag{A20}$$

The factor β has been introduced in the work by Sandorfi *et al.* [22] for consistency and it takes the value $\beta = \frac{1}{2}$ for observables which involve only beam and target polarization and $\beta = 1$ for quantities with recoil polarization. The unpolarized cross section σ_0 always assumes the form of the sum of the two polarization configurations:

$$\sigma_0 = \beta\left[\left(\frac{d\sigma}{d\Omega}\right)^{(B_1,T_1,R_1)} + \left(\frac{d\sigma}{d\Omega}\right)^{(B_2,T_2,R_2)}\right]. \tag{A21}$$

The dimensioned asymmetry $\sigma_0\mathcal{O}$ is often called a *profile function* [10,21] and is distinguished by a hat mark on the $\mathcal{O}$:

$$\hat{\mathcal{O}} = \beta\left[\left(\frac{d\sigma}{d\Omega}\right)^{(B_1,T_1,R_1)} - \left(\frac{d\sigma}{d\Omega}\right)^{(B_2,T_2,R_2)}\right]. \tag{A22}$$

For the photoproduction of a single pseudoscalar meson, there exist in total 16 polarization observables [22], which include also the unpolarized cross section σ_0 and which can be further

TABLE II. The definitions of the 16 polarization observables of pseudoscalar meson photoproduction in terms of transversity amplitudes b_i (cf. Ref. [21]) are collected here. Expressions are given both in terms of moduli and relative phases of the amplitudes and in terms of real- and imaginary parts of bilinear products of amplitudes. Furthermore, the phase-space factor ρ has been suppressed in the given expressions. The four different groups of observables are indicated as well. The sign-conventions for the observables are consistent with Ref. [10].

Observable	Group
$\sigma_0 = \frac{1}{2}(\lvert b_1\rvert^2 + \lvert b_2\rvert^2 + \lvert b_3\rvert^2 + \lvert b_4\rvert^2)$	
$\hat{\Sigma} = \frac{1}{2}(-\lvert b_1\rvert^2 - \lvert b_2\rvert^2 + \lvert b_3\rvert^2 + \lvert b_4\rvert^2)$	$\mathcal{S}$
$\hat{T} = \frac{1}{2}(\lvert b_1\rvert^2 - \lvert b_2\rvert^2 - \lvert b_3\rvert^2 + \lvert b_4\rvert^2)$	
$\hat{P} = \frac{1}{2}(-\lvert b_1\rvert^2 + \lvert b_2\rvert^2 - \lvert b_3\rvert^2 + \lvert b_4\rvert^2)$	
$\hat{E} = \mathrm{Re}[-b_3^* b_1 - b_4^* b_2] = -\lvert b_1\rvert\lvert b_3\rvert\cos\phi_{13} - \lvert b_2\rvert\lvert b_4\rvert\cos\phi_{24}$	
$\hat{F} = \mathrm{Im}[b_3^* b_1 - b_4^* b_2] = \lvert b_1\rvert\lvert b_3\rvert\sin\phi_{13} - \lvert b_2\rvert\lvert b_4\rvert\sin\phi_{24}$	$\mathcal{BT}$
$\hat{G} = \mathrm{Im}[-b_3^* b_1 - b_4^* b_2] = -\lvert b_1\rvert\lvert b_3\rvert\sin\phi_{13} - \lvert b_2\rvert\lvert b_4\rvert\sin\phi_{24}$	
$\hat{H} = \mathrm{Re}[b_3^* b_1 - b_4^* b_2] = \lvert b_1\rvert\lvert b_3\rvert\cos\phi_{13} - \lvert b_2\rvert\lvert b_4\rvert\cos\phi_{24}$	
$\hat{C}_{x'} = \mathrm{Im}[-b_4^* b_1 + b_3^* b_2] = -\lvert b_1\rvert\lvert b_4\rvert\sin\phi_{14} + \lvert b_2\rvert\lvert b_3\rvert\sin\phi_{23}$	
$\hat{C}_{z'} = \mathrm{Re}[-b_4^* b_1 - b_3^* b_2] = -\lvert b_1\rvert\lvert b_4\rvert\cos\phi_{14} - \lvert b_2\rvert\lvert b_3\rvert\cos\phi_{23}$	$\mathcal{BR}$
$\hat{O}_{x'} = \mathrm{Re}[-b_4^* b_1 + b_3^* b_2] = -\lvert b_1\rvert\lvert b_4\rvert\cos\phi_{14} + \lvert b_2\rvert\lvert b_3\rvert\cos\phi_{23}$	
$\hat{O}_{z'} = \mathrm{Im}[b_4^* b_1 + b_3^* b_2] = \lvert b_1\rvert\lvert b_4\rvert\sin\phi_{14} + \lvert b_2\rvert\lvert b_3\rvert\sin\phi_{23}$	
$\hat{L}_{x'} = \mathrm{Im}[-b_2^* b_1 - b_4^* b_3] = -\lvert b_1\rvert\lvert b_2\rvert\sin\phi_{12} - \lvert b_3\rvert\lvert b_4\rvert\sin\phi_{34}$	
$\hat{L}_{z'} = \mathrm{Re}[-b_2^* b_1 - b_4^* b_3] = -\lvert b_1\rvert\lvert b_2\rvert\cos\phi_{12} - \lvert b_3\rvert\lvert b_4\rvert\cos\phi_{34}$	$\mathcal{TR}$
$\hat{T}_{x'} = \mathrm{Re}[b_2^* b_1 - b_4^* b_3] = \lvert b_1\rvert\lvert b_2\rvert\cos\phi_{12} - \lvert b_3\rvert\lvert b_4\rvert\cos\phi_{34}$	
$\hat{T}_{z'} = \mathrm{Im}[-b_2^* b_1 + b_4^* b_3] = -\lvert b_1\rvert\lvert b_2\rvert\sin\phi_{12} + \lvert b_3\rvert\lvert b_4\rvert\sin\phi_{34}$	

divided into the four groups of single-spin observables ($\mathcal{S}$), beam-target ($\mathcal{BT}$), beam-recoil ($\mathcal{BR}$), and target-recoil ($\mathcal{TR}$) observables [21,24]. Each group is composed of four observables. When expressed in terms of the transversity amplitudes b_i, the 16 observables take the following form:

$$\hat{\mathcal{O}}^\alpha(W,\theta) = \frac{1}{2}\sum_{i,j=1}^{4} b_i^*(W,\theta)\Gamma_{ij}^\alpha b_j(W,\theta), \quad \alpha = 1,\ldots,16. \tag{A23}$$

The matrices Γ^α represent a complete and orthogonal set of 4×4 Dirac matrices, which are all by themselves Hermitian and unitary. Thus, the observables $\hat{\mathcal{O}}^\alpha$ are bilinear Hermitian forms in the transversity amplitudes. The matrices have been listed by Chiang and Tabakin [21] and can also be found in the Appendixes of the works [10]. Their algebraic properties imply useful quadratic constraints among the observables $\hat{\mathcal{O}}^\alpha$ known as the (generalized) *Fierz identities* [21]. A listing of the 16 quantities (A23) is expressed in terms of moduli $|b_i|$ and relative phases $\phi_{ij} := \phi_i - \phi_j$ of the transversity amplitudes in Table II.

APPENDIX B: CEA-AA AND TPWA

This Appendix compiles the definitions and mathematical details of both the complete-experiment analysis and amplitude analysis (CEA-AA) and the truncated partial-wave analysis (TPWA). Then, both methods are compared and the

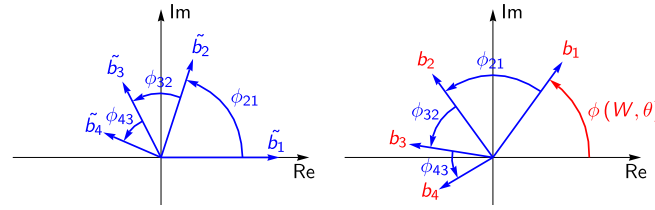

FIG. 18. The photoproduction amplitudes in the transversity basis are shown as an arrangement of four complex numbers. The schematic is taken over from Ref. [10]. The plots serve to illustrate the possible solutions of the CEA-AA. (left) The reduced amplitudes $\tilde{b}_i$, defined by the phase-constraint $\mathrm{Im}[\tilde{b}_1] = 0$, $\mathrm{Re}[\tilde{b}_1] \geqslant 0$, are plotted. A possible choice of three relative-phase angles is indicated. (right) The *true* solution for the actual transversity amplitudes b_i is shown and is obtained from the $\tilde{b}_i$ via a rotation by the overall phase $\phi(W,\theta)$ shown in red.

analysis-method proposed in this work emerges as a synergy of the two.

The CEA-AA represents the method to extract the four spin amplitudes, for instance, the transversity amplitudes $b_1,\ldots,b_4$, from a subset of the 16 observables collected in Table II. Due to the structure of the expressions (A23) as sums span over *bilinear amplitude products* $b_i^* b_j$, the amplitudes can only be extracted uniquely up to one unknown overall phase [5,21], which is a real function that can depend on the full reaction kinematics, i.e., on (W,θ). The final goal of the analysis is to obtain four amplitudes in the complex plane, with four uniquely defined moduli and three relative phase angles. This "rigid" amplitude arrangement is, however, free to rotate as a full entity in the complex plane with energy- and angle-dependent phase. See Fig. 18 for an illustration.

The choice of variables in terms of which to parametrize the amplitude arrangement is in principle not unique for the CEA-AA. Since one has four complex amplitudes and one unknown overall phase, the number of independent real variables in the choice always has to amount to $8-1=7$. Usually, one chooses four moduli of the b_i plus three suitably chosen relative phases, for instance,

$$|b_1|,\ |b_2|,\ |b_3|,\ |b_4|,\ \phi_{21},\ \phi_{32},\ \phi_{43}. \tag{B1}$$

However, in numeric data analyses, the parametrization in terms of moduli and relative phases can lead to difficulties caused by the logarithmic singularity which enters the procedure once complex exponentials have to be inverted. Alternatively, one can also think about parametrizing the CEA-AA in terms of the *phase-rotation functions* $e^{i\phi_{jk}}$, i.e., to use the set of variables

$$|b_1|,\quad |b_2|,\quad |b_3|,\quad |b_4|,\quad e^{i\phi_{21}} = \frac{|b_1|}{|b_2|}\frac{b_2}{b_1},$$
$$e^{i\phi_{32}} = \frac{|b_2|}{|b_3|}\frac{b_3}{b_2},\quad e^{i\phi_{43}} = \frac{|b_3|}{|b_4|}\frac{b_4}{b_3}. \tag{B2}$$

This removes the difficulty of having to invert exponentials. However, this is bought at the disadvantage of having increased the number of real degrees of freedom artificially, since the functions $e^{i\phi_{jk}}$ have both a real- and an imaginary part. Still, parametrizations in terms of phase-rotation func-

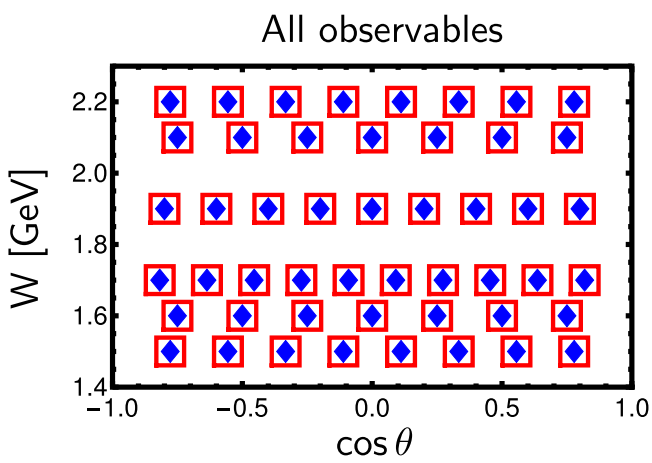

FIG. 19. A schematic illustration for a specific binning of points in phase space (blue polygons) for the CEA-AA. The kinematic binning has to agree for all observables. The CEA-AA then acts on each point individually (illustrated by the red boxes) and therefore all observables involved in the analysis have to be brought to the same binning.

tions are used in the main text (Sec. II) in order to "smooth" phase information coming from a PWA model.

Whatever choice one makes to parametrize the amplitudes, the CEA-AA is always a numerical (or algebraic) procedure which takes place at *one isolated point* in (W, θ) individually. This means that, in case one wishes to perform the CEA-AA for a collection of observables over a wider kinematic region, the kinematic binning of all these observables has to be brought to a match over this common region. The situation is illustrated in Fig. 19.

Consequently, the result of the CEA-AA, i.e., the seven variables parametrizing the transversity amplitudes with a fixed overall phase, is also returned as a set of "discrete data" in complex space. In other words, the standard CEA-AA without any constraints returns a discrete *but* not necessarily continuous set of points. The direct consequence is that partial waves with physical meaning cannot be extracted [9] without further imposing an overall phase provided by a theoretical model.

The TPWA denotes the procedure of extracting a finite set of photoproduction multipoles from experimental data by introducing continuous angular decomposition of amplitudes over Legendre polynomials. In practice, the multipole expansion defined by Eqs. (A12) to (A15) is truncated at some finite angular momentum $\ell_{\max}$. Inserting this truncation into the definitions of the 16 polarization observables shown in Table II yields the mathematical parametrization lying at the heart of the analysis.

The TPWA parametrization can be expressed in a concise form. Choosing to express the emerging angular dependence of the polarization observables $\hat{\mathcal{O}}^\alpha$ in terms of associated Legendre polynomials, one arrives at the following form (cf. Refs. [10,25–27]):

$$\hat{\mathcal{O}}^\alpha(W,\theta) = \frac{q}{k} \sum_{n=\beta_\alpha}^{2\ell_{\max}+\beta_\alpha+\gamma_\alpha} (a_L)_n^{\hat{\mathcal{O}}^\alpha}(W) P_n^{\beta_\alpha}(\cos\theta), \quad \alpha = 1,\ldots,16, \tag{B3}$$

$$(a_L)_n^{\hat{\mathcal{O}}^\alpha}(W) = \left\langle \mathcal{M}_{\ell_{\max}}(W) \right| (\mathcal{C}_L)_n^{\hat{\mathcal{O}}^\alpha} \left| \mathcal{M}_{\ell_{\max}}(W) \right\rangle. \tag{B4}$$

The *Legendre coefficients* $(a_L)_n^{\hat{\mathcal{O}}^\alpha}$ take on bilinear Hermitian forms defined by a certain set of matrices $(\mathcal{C}_L)_n^{\hat{\mathcal{O}}^\alpha}$ (such matrices are given explicitly for the group $\mathcal{S}$ and $\mathcal{BT}$ observables in the Appendix of Ref. [10]). The multipoles are organized into the $4\ell_{\max}$-dimensional complex vector $|\mathcal{M}_{\ell_{\max}}\rangle$ according to the convention

$$\left|\mathcal{M}_{\ell_{\max}}\right\rangle = [E_{0+}, E_{1+}, M_{1+}, M_{1-}, E_{2+}, E_{2-}, \ldots, M_{\ell_{\max}-}]^T. \tag{B5}$$

The quantities β_α and γ_α in Eqs. (B3) and (B4) are constants which define the precise form of the TPWA for each observable. These constants can be found, for instance, in Refs. [10,27].

For the TPWA, all observables have to be prepared with a common energy binning. However, since this method for extracting amplitudes actually parametrizes the angular dependence continuously [cf. Eq. (B3)], the angular binnings of the observables can be different. The TPWA then returns a continuous function in angle for each of the discrete energy bins. However, continuity in energy is another matter and has been discussed elsewhere [5]. The kinematic situation is illustrated in Fig. 20.

Note that the CEA-AA and the TPWA *are not* equivalent procedures and will not lead to identical results. This becomes especially apparent once one compares the *complete sets of observables* [21,28], i.e., minimal subsets of all polarization observables which allow for an unambiguous extraction of the complex amplitudes (or multipoles), valid for both analysis procedures. The differences among and the most important characteristics of the CEA-AA and the TPWA are listed in the following:

CEA-AA (i) Kinematic regime: the CEA-AA takes place at individual points in the two-dimensional space (W, θ) spanned by the energy W and scattering angle θ.

(ii) In the CEA-AA, one has four complex amplitudes while one overall phase $\phi(W, \theta)$ is not known. This results in $8 - 1 = 7$ real independent variables.

(iii) A mathematical complete set for the CEA-AA is given by eight carefully chosen observables [21,29]. In addition to the four observables from the group $\mathcal{S}$ (cf. Table II), one has to select four double polarization observables which must not belong to the same group. This becomes apparent once one considers, for instance, the 4 $\mathcal{BT}$ observables listed in Table II: all four observables only contain information on two relative phases, ϕ_{13} and ϕ_{24}. Thus, even if all $\mathcal{BT}$ observables were measured, at least one connecting relative phase, for instance ϕ_{12}, remains unknown, which results in a continuous ambiguity. Therefore, at least two observables must be chosen from a third group, e.g.,

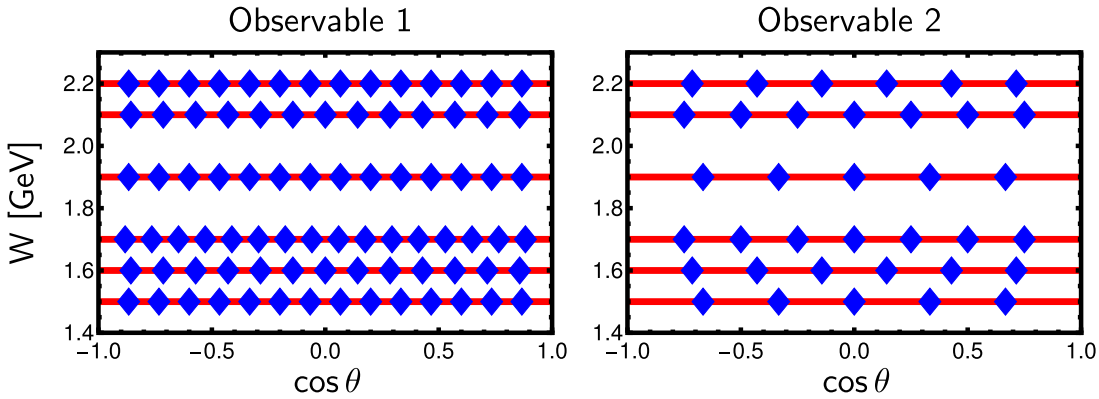

FIG. 20. The plots show schematic illustrations for the kinematic situation in the TPWA. Figures are shown for two different hypothetical observables. Further observables are not shown, but surely present in the TPWA. The kinematic binning for all the data points (blue polygons) does not have to fully agree between all observables. However, the energy binning has to be the same for all datasets. The TPWA (represented by red solid lines) introduces a continuous dependence on the angular variable $\cos\theta$. Compare this to Fig. 19.

the $\mathcal{BR}$ observables. Further rules for the selection of complete sets can be found in Refs. [21,29].

Recent studies [30–33] demonstrate the fact that the completeness of the minimal complete sets of eight is lost once measurement errors of realistic sizes are introduced. Then, in order to recover a unique solution for the amplitudes, the considered complete set of eight has to be enlarged.

(iv) In case a mathematically *in*complete set of observables has been selected for the CEA-AA, in most cases this results in only an additional twofold discrete ambiguity (in case the four double-polarization measurements are not taken from the same group).

(v) In a world without measurement uncertainties, the CEA-AA yields an exact representation of the photoproduction $\mathcal{T}$ matrix (up to one overall phase). This is accomplished by extracting four complex numbers, independently of the considered energy region. The phase of one of the four complex numbers has to be constrained, e.g., by demanding this number to be real and positive.

TPWA (i) Kinematic regime: the TPWA is performed at an individual point in W, but over a whole distribution in the angular variable θ (or $\cos\theta$).

(ii) In the TPWA, one has $4\ell_{\max}$ complex multipoles while one energy-dependent overall phase $\phi(W)$ is not known. This results in $8\ell_{\max}-1$ real independent variables in case the phase $\phi(W)$ is fixed in some way.

(iii) A mathematical complete set for the TPWA is given by minimally four observables [9,10]. However, these complete sets of four can only be found in numerical simulations. On the other hand, an algebraic solution theory exists for complete sets composed of five carefully chosen observables [10,26,28,34]. The minimal mathematical complete sets mentioned here lose their validity once measurement errors of realistic sizes are introduced (cf. Sec. 5.5 of Ref. [10]) and then have to be enlarged in order to facilitate a unique solution.

(iv) In case a mathematically *in*complete set of observables has been selected for the TPWA, one obtains an exact twofold discrete ambiguity called a *double ambiguity* [10,28,34], but also a number of (possible) approximate *accidental ambiguities* exists, which scales as $4^{2\ell_{\max}}-2$ [10,34]. These discrete ambiguities can cause severe stability problems for TPWAs performed with higher truncation orders, i.e., $\ell_{\max}>2$ (cf. the Appendixes of Ref. [10]).

(v) In a world without measurement uncertainties, the TPWA already contains an inherent systematic error due to the fact that it only yields an *approximation* of the photoproduction $\mathcal{T}$ matrix for any finite $\ell_{\max}$. For higher energies, one generally has to choose a higher truncation order $\ell_{\max}$, which can result in an increased numerical instability.

In this work, we combine both analysis-procedures and use the amplitudes resulting from a CEA-AA in order to resolve the instability problems of the TPWA, which exist mainly for higher truncation orders.

As explained in detail in the main text (Sec. II), a CEA-AA with smooth, analytic phases originating from a theoretical model is used as a penalty function in the two-step process in order to ensure the continuity and to increase the stability of the TPWA. In this way, the advantages of both methods have been combined, and a synergy is created which produces a reliable and very precise description of the data, while at the same time additional theoretical requirements like a good threshold behavior are obeyed.

[1] M. Tanabashi *et al.* (Particle Data Group), Phys. Rev. D **98**, 030001 (2018).

[2] D. Atkinson, P. W. Johnson, and R. L. Warnock, Commun. Math. Phys. **33**, 221 (1973).

[3] J. E. Bowcock and H. Burkhard, Rep. Prog. Phys. **38**, 1099 (1975).

[4] D. Atkinson and I. S. Stefanescu, Commun. Math. Phys. **101**, 291 (1985).

[5] A. Švarc, Y. Wunderlich, H. Osmanović, M. Hadžimehmedović, R. Omerović, J. Stahov, V. Kashevarov, K. Nikonov, M. Ostrick, L. Tiator, and R. Workman, Phys. Rev. C **97**, 054611 (2018).

[6] Y. Wunderlich, A. Švarc, R. L. Workman, L. Tiator, and R. Beck, Phys. Rev. C **96**, 065202 (2017).

[7] G. Höhler, Pion nucleon scattering, in Part 2 of *Landolt-Bornstein: Elastic and Charge Exchange Scattering of Elementary Particles* (Springer-Verlag, Berlin, 1983), Vol. 9b.

[8] H. Osmanović, M. Hadžimehmedović, R. Omerović, J. Stahov, V. Kashevarov, K. Nikonov, M. Ostrick, L. Tiator, and A. Švarc, Phys. Rev. C **97**, 015207 (2018).

[9] R. L. Workman, L. Tiator, Y. Wunderlich, M. Döring, and H. Haberzettl, Phys. Rev. C **95**, 015206 (2017), and references therein.

[10] Y. Wunderlich, Ph.D. thesis, University of Bonn, 2020, arXiv:2008.00514.

[11] R. L. Workman, M. W. Paris, W. J. Briscoe, L. Tiator, S. Schumann, M. Ostrick, and S. S. Kamalov, Eur. Phys. J. A **47**, 143 (2011).

[12] A. V. Anisovich *et al.*, Phys. Rev. C **96**, 055202 (2017), and references therein.

[13] A. Sarantsev *et al.*, Bonn Gatchina Partial Wave Analysis, https://pwa.hiskp.uni-bonn.de/.

[14] A. Švarc, M. Hadžimehmedović, H. Osmanović, J. Stahov, L. Tiator, and R. L. Workman, Phys. Rev. C **88**, 035206 (2013), and references therein.

[15] E. F. McNicoll *et al.* (Crystal Ball at MAMI Collaboration), Phys. Rev. C **82**, 035208 (2010); **84**, 029901(E) (2011).

[16] O. Bartalini *et al.* (GRAAL Collaboration), Eur. Phys. J. A **33**, 169 (2007).

[17] J. R. M. Annand *et al.* [A2 and MAMI Collaborations], Phys. Rev. C **93**, 055209 (2016).

[18] J. Müller *et al.* (CBELSA/TAPS Collaboration), Phys. Lett. B **803**, 135323 (2020).

[19] J. Landay, M. Döring, C. Fernández-Ramírez, B. Hu and R. Molina, Phys. Rev. C **95**, 015203 (2017).

[20] G. F. Chew, M. L. Goldberger, F. E. Low, and Y. Nambu, Phys. Rev. **106**, 1345 (1957).

[21] W. T. Chiang and F. Tabakin, Phys. Rev. C **55**, 2054 (1997).

[22] A. M. Sandorfi, S. Hoblit, H. Kamano, and T.-S. H. Lee, J. Phys. G **38**, 053001 (2011).

[23] J. S. Ball, Phys. Rev. **124**, 2014 (1961).

[24] I. S. Barker, A. Donnachie, and J. K. Storrow, Nucl. Phys. B **95**, 347 (1975).

[25] L. Tiator, AIP Conf. Proc. **1432**, 162 (2012).

[26] V. F. Grushin, in *Photoproduction of Pions on Nucleons and Nuclei*, edited by A. A. Komar (Nova Science, New York, 1989), p. 1ff.

[27] Y. Wunderlich, F. Afzal, A. Thiel, and R. Beck, Eur. Phys. J. A **53**, 86 (2017).

[28] Y. Wunderlich, R. Beck, and L. Tiator, Phys. Rev. C **89**, 055203 (2014).

[29] K. Nakayama, Phys. Rev. C **100**, 035208 (2019).

[30] T. Vrancx, J. Ryckebusch, T. Van Cuyck, and P. Vancraeyveld, Phys. Rev. C **87**, 055205 (2013).

[31] T. Vrancx, J. Ryckebusch, and J. Nys, EPJ Web Conf. **73**, 04011 (2014).

[32] J. Nys, T. Vrancx, and J. Ryckebusch, J. Phys. G **42**, 034016 (2015).

[33] D. G. Ireland, Phys. Rev. C **82**, 025204 (2010).

[34] A. S. Omelaenko, Yad. Fiz. **34**, 730 (1981) [Sov. J. Nucl. Phys. **34**, 406 (1981)].